1-d Model for Propagation and Absorption of h.f. Waves Near Ion Cyclotron Resonances in Large Tokamak Plasmas

T. Krücken

IPP 5/9 Mai 1986

MAX-PLANCK-INSTITUT FÜR PLASMAPHYSIK

8046 GARCHING BEI MÜNCHEN

MAX-PLANCK-INSTITUT FÜR PLASMAPHYSIK

GARCHING BEI MÜNCHEN

1-d Model for Propagation and Absorption of h.f. Waves Near Ion Cyclotron Resonances in Large Tokamak Plasmas

T. Krücken

IPP 5/9 Mai 1986

Die nachstehende Arbeit wurde im Rahmen des Vertrages zwischen dem Max-Planck-Institut für Plasmaphysik und der Europäischen Atomgemeinschaft über die Zusammenarbeit auf dem Gebiete der Plasmaphysik durchgeführt.

1-d Model for Propagation and Absorption of h.f. Waves Near Ion Cyclotron Resonances in Large Tokamak Plasmas

T. Krücken

IPP 5/9

Abstract

The behaviour of h.f. waves near ion cyclotron and ion ion hybrid resonances in a tokamak is investigated by means of an onedimensional finite element code. Our model takes into account:

- strength and orientation of the poloidal component of the static magnetic field,
- finite larmor radius corrections to the dielectric tensor,
- ion cyclotron damping at the fundamental and first harmonic resonance,
- electron Landau damping to lowest order m_e/m_i.

We assume that an incoming fast wave approaches the singular layer from the low or high field side making an arbitrary angle relative to the local magnetic flux surface and to the resonance layer. These initial conditions might be provided by ray tracing from the antenna. Then we calculate the electromagnetic wavefield and the power fluxes of the transmitted or reflected fast and slow waves as well as the power absorbed by ions and electrons.

1. Introduction

Ray tracing /1/ has proven an attractive tool for modelling ICRF heating of large plasma. To be really useful, however, it has to be supplemented by the full wave analysis near ion cyclotron and ion ion hybrid resonances where the WKB method fails, In this region the dielectric tensor depends almost only on the strength of the static magnetic field which is basically a function of the horizontal coordinate x. Hence the wave equation can be approximated by an onedimensional differential equation /2,3/ assuming that n and K_z, the toroidal and vertical wave vector components, remain constant within the singular layer. Further details of this model will be outlined in section 2. In section 3 we shall discuss the properties of the dielectric tensor in the "warm plasma" approximation /4,5,6/ and the difficulties arising from the nonlocal character of the various kinetic damping processes (ion cyclotron damping, ICD; electron transit time damping, TTMP; electron Landau damping, ELD). Existing analytical approaches /3,7/ to solve the resulting differential equation rely on the assumption that the region of mode conversion lies outside the layer of strong cyclotron damping which is not always justified. They are also not able to treat in all generality the important scenario of a hydrogen minority in a deuterium plasma where the ion ion hybrid resonance is very close to the majority's first harmonic resonance. Therefore we have written a numerical code which we shall describe in section 5 after a discussion of the dispersion relation /8/ in section 4. In section 6 we shall apply our code to various heating scenarios and compare the results with those from the analytical models mentioned above.

2. An approximate 1-d wave equation for the e.m. field near a resonance layer

For a wave with time dependence exp(-iωt) Maxwell equations can be written:

$$\mathrm{rot}\,\mathrm{rot}\,\vec{E} = \frac{\omega^2}{c^2}\left(\vec{E} + \frac{4\pi i}{\omega}\vec{j}\right) = \hat{\underline{\varepsilon}}\,\vec{E} \qquad (1)$$

where $\vec{J}(\vec{E})$ is the h.f. current in the plasma. We shall refer to $\hat{\underline{\varepsilon}}$ in the following as the "dielectric tensor" although it is, strictly speaking, a linear, nonlocal integraloperator. In the vicinity of a resonance eq. (1) is dominated by the strong variations of $\hat{\underline{\varepsilon}}$ due to the horizontal gradient of the static magnetic field $\vec{B}$:

$$|\vec{B}| \simeq B_0 \cdot \frac{R_T}{X} \qquad (2)$$

R_T denoting the major plasma radius, X the horizontal coordinate. Hence we make the ansatz

$$\vec{E} = \vec{E}(x) \cdot e^{i(m_\varphi \varphi + K_z z)} \qquad (3)$$

with the toroidal mode number n_φ and the vertical component of the wave vector K_Z being constant. As anticipated from the next section, $\hat{\underline{\varepsilon}}$ is most conventiently expressed using rotating coordinates with respect to $\vec{B}$ decomposing $\vec{E}$ in its left (E_+) and right (E_-) circularly polarised component and $E_\parallel$ parallel to $\vec{B}$. In a tokamak $\vec{B}$ is approximately given by:

$$\vec{B} = |\vec{B}| \cdot \left[\cos\theta\,\vec{e}_\varphi + \sin\theta\,(\cos\tau\,\vec{e}_z - \sin\tau\,\vec{e}_x)\right] \qquad (4)$$

where $\tan\theta = B^{Pol}/B_{tor} \simeq$ const in the region of interest. The angle τ is visualized in fig. 1. In our model we assume that τ is constant in the vicinity of a resonance, i.e. we neglect the curvature of magnetic flux surfaces. This is probably the severest simplification. For example, the slow wave, being excited due to mode conversion near a resonance, tends to propagate along flux surfaces.

Nevertheless, for large tokamaks like JET, $\tau \simeq$ const is an acceptable approximation because the interval where we solve eq. (1) is very small compared to the device size.

Using eq. (3) and eq. (4) we can write the rot rot operator in our reference frame:

$$
\begin{aligned}
(\mathrm{rot}\,\mathrm{rot}\,\vec{E})_+ &= -(\partial_+\partial_- + \partial_\parallel^2)E_+ + \partial_+\partial_+ E_- + \partial_+(\partial_\parallel E_\parallel) \\
(\mathrm{rot}\,\mathrm{rot}\,\vec{E})_- &= -(\partial_+\partial_- + \partial_\parallel^2)E_- + \partial_-\partial_- E_+ + \partial_-(\partial_\parallel E_\parallel) \qquad (5) \\
(\mathrm{rot}\,\mathrm{rot}\,\vec{E})_\parallel &= -2\partial_+\partial_- E_\parallel + \partial_\parallel(\partial_+ E_- + \partial_- E_+)
\end{aligned}
$$

where

$$
\begin{aligned}
\partial_\parallel &= i\frac{n_\varphi}{R_0}\cos\theta + i\sin\theta\cos\tau\, K_z - \sin\theta\sin\tau\,\frac{d}{dx} \\
\partial_\pm &= \frac{1}{\sqrt{2}}\left\{\left[\cos\tau\,\frac{d}{dx} + i\sin\tau\, K_z\right]\right. \qquad (6) \\
&\left. \pm i\left[-\cos\theta\sin\tau\,\frac{d}{dx} + i\cos\theta\cos\tau\, K_z - i\sin\theta\,\frac{n_\varphi}{R_0}\right]\right\}
\end{aligned}
$$

with R_0 denoting the position of the cyclotron resonance as shown in fig. 1. In the next section, we shall discuss the other part of eq. (1) the generalized dielectric tensor .

3. The dielectric tensor

Brambilla and Ottaviani /6/ have, based on works by Swanson /4/ and by Colestock and Kashuba /5/, derived the dielectric tensor $\hat{\underline{\underline{\varepsilon}}}$ by integrating the linearized Vlasov equation along unperturbed particle trajectories. In the "warm plasma" approximation it contains full parallel dispersion and perpendicular dispersion to second order Larmor radius (FLR-corrections). In zero order Larmor radius obtains:

$$(\hat{\underline{\underline{\varepsilon}}}^{(0)}\vec{E}) = (L E_+)\vec{e}_+ + R E_- \vec{e}_- + (P E_\parallel)\vec{e}_\parallel \qquad (7)$$

with

$$(L E_+)(x,z,\varphi) = \left(1 + \frac{\omega_{pe}^2}{\Omega_{ce}^2}\left(1 - \frac{\Omega_{ce}}{\omega}\right)\right) E_+(x,z,\varphi)$$

$$+ \sum_{ions} \frac{\omega_{pi}^2}{\omega^2} \int dv_\parallel \frac{e^{-v_\parallel^2/v_{thi}^2}}{\sqrt{\pi}\, v_{thi}} \left[i\omega \int_0^\infty dt\, e^{i(\omega - \Omega_c)t} E_+(x'(t), z'(t), \varphi'(t)) \right] \qquad (8)$$

$$R E_-(x,z,\varphi) = \left[1 + \frac{\omega_{pe}^2}{\Omega_{ce}^2}\left(1 + \frac{\Omega_{ce}}{\omega}\right) - \sum_{ions} \frac{\omega_{pi}^2}{\omega^2} \frac{\omega}{\omega + \Omega_{ci}}\right] E_-(x,z,\varphi)$$

$$P E_\parallel(x,z,\varphi) = -\frac{\omega_{pe}^2}{\omega^2} \int dv_\parallel \frac{e^{-v_\parallel^2/v_{the}^2}}{\sqrt{\pi}\, v_{the}} \left[i\omega \int_0^\infty dt\, e^{i\omega t} \cdot E_\parallel(x'(t), z'(t), \varphi'(t)) \right]$$

where $v_{th}, \omega_p, \Omega_c$ denote a species thermal velocity, plasma frequency and cyclotron frequency, respectively, and:

$$x'(t) = x + v_\parallel \sin\theta \sin\tau \cdot t$$

$$z'(t) = z - v_\parallel \sin\theta \cos\tau \cdot t$$

$$\varphi'(t) = \varphi - \frac{v_\parallel}{R_0} \cos\theta \cdot t$$

The FLR-corrections are given by:

$$\left(\hat{\underline{\underline{\xi}}}^{(2)}\vec{E}\right)_+ = 2\,\partial_-\lambda_2\partial_+ E_+ + 2\partial_+\lambda_0\left(\partial_- E_+ - \partial_+ E_-\right)$$

$$\left(\hat{\underline{\underline{\xi}}}^{(2)}\vec{E}\right)_- = 2\,\partial_-\lambda_0\left(\partial_+ E_- - \partial_- E_+\right) \qquad (9)$$

with $\partial_\pm$ as defined in eq. (6) and

$$(\lambda_0 E_\pm)(x,z,\varphi) = \frac{1}{2}\frac{\omega_{pe}^2}{\Omega_{ce}^2}\frac{v_{the}^2}{c^2}\int dv_\parallel \frac{e^{-v_\parallel^2/v_{the}^2}}{\sqrt{\pi}\,v_{the}} \cdot\left[i\omega\int_0^\infty dt\, e^{i\omega t} E_\pm(x'(t),z'(t),\varphi'(t))\right]$$

$$(\lambda_2 E_+)(x,z,\varphi) = \frac{1}{2}\sum_i \frac{\omega_{pi}^2}{\Omega_{ci}^2}\frac{v_{thi}^2}{c^2}\int dv_\parallel \frac{e^{-v_\parallel^2/v_{thi}^2}}{\sqrt{\pi}\,v_{thi}} \left[i\omega\int_0^\infty dt\, e^{i(\omega-2\Omega_{ci})t} E_+(x'(t),z'(t),\varphi'(t))\right] \qquad (10)$$

L and λ_2 are resonant at $\omega=\Omega_c$ and $\omega=2\Omega_c$, respectively. Their antihermitean parts describe ICD at the fundamental and first harmonic resonance, the one of P and λ_0 ELD and TTMP, respectively. P and λ_0, as well as L and λ_2 near their resonances, are non-local integral operators. Assuming that the spatial dependence of the e.m. field parallel to the static magnetic field is $\sim e^{ik_\parallel x_\parallel}$ with a given $k_\parallel$, one can evaluate the integrals and finds the algebraic expressions:

$$L = 1 + \frac{\omega_{pe}^2}{\Omega_{ce}^2} - \sum_i\left[-x_{0,i}\,Z(x_{1,i}) + \frac{\omega}{\Omega_{ci}}\right]$$

$$P = 1 - \frac{\omega_{pe}^2}{\Omega_{ce}^2}\,x_{0,e}\,Z'(x_{0,e})$$

$$\lambda_0 = -\frac{1}{2}\frac{\omega_{pe}^2}{\Omega_{ce}^2}\frac{v_{the}^2}{c^2}\,x_{0,e}\,Z(x_{0,e}) \qquad (11)$$

$$\lambda_2 = -\frac{1}{2}\sum_i \frac{\omega_{pi}^2}{\Omega_{ci}^2}\frac{v_{thi}^2}{c^2}\,x_{0,i}\,Z(x_{2,i})$$

with $$X_{n,i} = \frac{\omega - n\,\Omega_{c_i}(x)}{K_{\parallel}\, v_{th_i}}$$

and $$Z(x) = \frac{1}{\sqrt{\pi}} \int \frac{e^{-u^2}}{u-x}\,du + i\sqrt{\pi}\,\frac{K_{\parallel}}{|K_{\parallel}|}\,e^{-x^2}$$

denoting the Fried-Conte Zetafunction /9/. In tokamak geometry, however, this is strictly speaking not possible since the non-vanishing poloidal component of the magnetic field doesn't allow for a well defined $K_{\parallel}$. In our model, $K_{\parallel}$ would be given by

$$K_{\parallel} = \frac{n_\varphi}{R_0}\cos\theta + \sin\theta\,(\cos\tau\,K_z - \sin\tau\,K_x) \qquad (12)$$

with K_x unknown.

But for those damping processes localized near a resonance (ICD) or which affect only the transversal fast waves (TTMP) it is adequate to neglect the last term in eq. (11) since $\frac{n_\varphi}{R_0}\cos\theta \gg \sin\theta\,K_x|_{fast}$ holds for most values of the toroidal mode number n_φ . Furthermore, dropping this term is acceptable near the equatorial plane where $\sin\tau \simeq 0$. To describe ELD, however, which hardly affects the transversal fast waves, whereas it is the most important damping mechanism for the longitudinal, electrostatic slow waves, one has to make another approximation. In calculating P we have therefore used the expression:

$$K_{\parallel,s} \simeq \frac{n_\varphi}{R_0}\cos\theta + \sin\theta\,(\cos\tau\,K_z - \sin\tau\,K_{x|_{slow}}) \qquad (13)$$

where $K_{x|_{slow}}$ is an estimate of the solution of the dispersion relation for outgoing slow waves (see next chapter).

Another problem arises from the different orders of magnitude of $E_{\pm}$ and $E_{\parallel}$: Because of the very low electron inertia, P is much larger than the other tensor elements. Hence $E_{\parallel}$ is of order m_e/m_i smaller than $E_{\pm}$. In order to avoid scale problems one usually sets $E_{\parallel} \equiv 0$. By taking this zero electron inertia limit, however, ELD is lost. Therefore we use the parallel component of eq. (1) to express $E_{\parallel}$ in terms of $E_{\pm}$ retaining only terms to lowest order m_e/m_i :

$$E_{\parallel} \simeq \frac{1}{P}\,\partial_{\parallel}\,(\partial_{+}E_{-} + \partial_{-}E_{+}) \tag{14}$$

and insert this expression in the other two equations. This allows us to eliminate $E_{\parallel}$ without omitting ELD, but increases the order of our differential equation by 2. Since the resulting new wave is always evanescent, however, it is justified to replace in the corresponding terms $\partial_{\parallel}$ by $i\,K_{\parallel,S}$.

To summarize the results of this and the previous section we rewrite the complete onedimensional wave equations:

$$\begin{aligned}
&-(\partial_{+}\partial_{-}+\partial_{\parallel}^{2})E_{+} + \partial_{+}\partial_{+}E_{-} - \partial_{+}\frac{K_{\parallel,S}^{2}}{P}(\partial_{+}E_{-}+\partial_{-}E_{+}) \\
&= L E_{+} + 2\partial_{-}\lambda_{2}\partial_{+}E_{+} + 2\partial_{+}\lambda_{0}(\partial_{-}E_{+} - \partial_{+}E_{-})\,; \\
&-(\partial_{+}\partial_{-}+\partial_{\parallel}^{2})E_{-} + \partial_{-}\partial_{-}E_{+} - \partial_{-}\frac{K_{\parallel,S}^{2}}{P}(\partial_{+}E_{-}+\partial_{-}E_{+}) \\
&= R E_{-} \qquad\qquad + 2\partial_{-}\lambda_{0}(\partial_{+}E_{-} - \partial_{-}E_{+})
\end{aligned} \tag{15}$$

Since we are interested only in the behaviour near a singular layer we assume that all quantities except L(X) and λ_2(X) which might be resonant, remain constant over the interval.

4. The dispersion relation

Before explaining the numerical method used to solve this system of two coupled second order differential equations, we want to draw some information from the dispersion relation /8/. Upon replacing in eq. (15) $\frac{d}{dx}$ by iK_X we obtain the local dispersion relation. With

$$\begin{aligned}
\Diamond &= \alpha^{2}K_{x}^{2} - 2\beta K_{x} - \vartheta \\
\alpha &= \sin\theta\,\sin\tau \\
\beta &= \sin\theta\,\sin\tau\left(\frac{n_{\varphi}}{R_0}\cos\theta - K_{z}\sin\theta\cos\tau\right) \\
-\vartheta &= 2\sin\theta\cos\theta\cos\tau\,\frac{n_{\varphi}}{R_0}K_{z} - \sin^{2}\theta\left(\frac{n_{\varphi}^{2}}{R_0^{2}} - K_{z}^{2}\cos^{2}\tau\right)
\end{aligned} \tag{16}$$

and $K_{\perp_0}^2 = K_X^2 + K_Z^2$ it reads:

$$K_{\perp_0}^2 \nu\left(1+2\lambda_0-\frac{K_{\parallel,S}^2}{P}\right)+\frac{\lambda_2}{2}K_{\perp_0}^2+\frac{K_{\parallel,S}^2}{P}K_{\perp_0}^4$$
$$+\left(\frac{n_\varphi^2}{R_0^2}-S\right)\left(\left(K_{\perp_0}^2+\nu\right)+\left(K_{\perp_0}^2-\nu\right)\left(\lambda_0+\frac{K_{\parallel,S}^2}{P}\right)\right) \qquad (17)$$
$$+\lambda_2\left(\frac{n_\varphi^2}{R_0^2}-R\right)\left(K_{\perp_0}^2-\nu\right)+\left(\frac{n_\varphi^2}{R_0^2}-L\right)\left(\frac{n_\varphi^2}{R_0^2}-R\right)=0$$

where we have neglected terms proportional to ν^2 ($\sim \sin^2\theta$) and $\nu\cdot\lambda_2$.

The roots of eq. (17) are approximately given by:

$$K_x^2\big|_{fast} \simeq -K_z^2-\frac{(K_{\parallel_0}^2-L)(K_{\parallel_0}^2-R)}{(K_{\parallel_0}^2-S)} \qquad (18)$$

$$K_x^2\big|_{slow} \simeq \frac{S}{\lambda_2/2+\alpha^2} \qquad (19)$$

where $K_{\parallel_0}=\frac{n_\varphi}{R_0}+\sin\theta\cos\cdot K_Z$; $S=\frac{R+L}{2}$.

Eq. (17) describes the fast, magnetosonic wave which is usually excited by the antenna. It encounters a cutoff for $L = K_{\parallel_0}^2 \simeq 0$. For a two-component plasma its position can be given by:

$$X_{c.o.} = X_{Res}+\nu_2 Z_2\left(\frac{Z_1/A_1}{Z_2/A_2}-1\right) \qquad (20)$$

X_{Res} is the position of the minority's fundamental resonance (= R_0 in our model), $\nu_i = n_i/n_e$ denote the concentrations, Z_i and A_i the atomic charge- and massnumbers of the two ions. The position of the socalled hybrid resonance, $S = K_{\parallel_0}^2 \simeq 0$ for a two component plasma is

$$X_{hyb} = X_{Res}\sqrt{\frac{1+\nu_2 Z_2\left(\frac{Z_1/A_1}{Z_2/A_2}-1\right)}{1+\nu_2 Z_2\left(\frac{Z_2/A_2}{Z_1/A_1}-1\right)}} \qquad (21)$$

At this point, mode conversion to the other branch of the dispersion relation, the slow wave, occurs: In the vicinity of $\omega \simeq 2\Omega_c$ eq. (19) describes the ion Bernstein wave. One property of this wave is that it runs backwards, i.e. power flux and phase velocity point in opposite directions.

For $\mathcal{L}_2 \approx 0$ eq. (19) describes the cold plasma shear Alfvén or ion cyclotron wave. This wave exists only for nonvanishing poloidal magnetic field. Hence it is necessary to retain FLR-corrections as well as B^{Pol} to describe the slow wave properly.

Mode conversion to the ion Bernstein wave can also occur in a single species plasma near the second harmonic resonance /10/. The positions of cutoff of the fast wave and confluence are approximately given by:

$$X_{c.o.} - X_{Res} = -\frac{\omega_p^2}{\Omega_c^2}\frac{v_{th}^2}{c^2} X_{Res}\left(1-\frac{\sqrt{3}}{2}\right) \qquad (22)$$

$$X_{conf} - X_{Res} = -\frac{\omega_p^2}{\Omega_c^2}\frac{v_{th}^2}{c^2} X_{Res}\left(1+\frac{\sqrt{3}}{2}\right) \qquad (23)$$

Here, X_{Res} denotes the position of the second harmonic resonance (= R_o in our model).

Eq. (19) has been used in our code to estimate $K_{X/slow}$ in eq. (13) for the $K_{\parallel,S}$ of outgoing slow waves taking into account that the ion Bernstein wave runs backwards.

At each side of the interval we have solved the dispersion relation (17) numerically by means of a Newton iteration taking eq. (18) and (19) as start values. The resulting wave-vector components K_X and polarisations

$$W = \frac{E_-}{E_+} = \Big[(1+\alpha^2)K_x^2 - 2\beta K_x + K_z^2 - \gamma + 2\left(\frac{n\xi}{R_o^2} - L\right) + \left((1-\alpha^2)K_x^2 + 2\beta K_x + K_z^2 + \gamma\right)\left(2\mathcal{L}_2 + 2\mathcal{L}_0 + \frac{K_{\parallel,S}^2}{p}\right)\Big] \Big/ \qquad (24)$$

$$\Big/ \Big[(v + u K_z)^2\left(1 + 2\mathcal{L}_0 - \frac{K_{\parallel,S}}{p}\right)\Big]$$

with

$$u = \cos\tau - i\cos\theta \sin\tau ;$$

$$v = K_z \sin\tau + i\left(K_z \cos\theta \cos\tau - \sin\theta \frac{n\varphi}{R_o}\right) \quad (25)$$

of the fast and slow waves are needed to impose the radiation conditions at the boundaries as we shall explain in the next section.

5. Solving the wave equation

5.1 Determination of the interval

As mentioned in the introduction the code is intended to be coupled to a ray tracing code to solve the wave equation near resonances where mode conversion is expected. Hence the WKB approximation should be valid at both ends X_A and X_B of the interval. In case of a single component plasma, where the interval is centered at the second harmonic resonance ($R_o = X_{Res} = x\ (\omega = 2\Omega_c)$) we choose

$$X_{A,B} = X_{Res} \pm 6\left(X_{Conf} - X_{Res}\right)$$

X_{conf} denoting the position of confluence as obtained from eq. (21).

In case of a two component plasma the interval is centered at the minority's fundamental resonance ($R_o = X_{Res} = X(\omega = \Omega_{c_{Min}})$) and we impose the conditions:

$$|X_A - X_{Res}| = |X_B - X_{Res}| > 3\,|X_{hyb} - X_{Res}|$$

with X_{hyb} given by Eq. (21). The minority's contribution to L at the ends X_A and X_B must be smaller than 20 % and

$$\frac{Im(L)}{Re(L)} < 10^{-20} \quad \text{at } X_A, X_B$$

5.2 Determination of the mesh

One advantage of the finite element method is that it doesn't require an equidistant mesh. Hence we have adjusted the resolution of the mesh to the local properties of the expected solution by imposing the following conditions:

$$\frac{L(X_{i+1}) - L(X_i)}{L(X_i)} < 0.2 \qquad \text{(a)}$$

$$\frac{\mathcal{Z}_2(X_{i+1}) - \mathcal{Z}_2(X_i)}{\mathcal{Z}_2(X_i)} < 0.2 \qquad \text{(b)}$$

$$X_{i+1} - X_i < \frac{1}{5 \cdot \sqrt{R}} \qquad \text{(c)}$$

$\sqrt{R}$ being an estimate of $K_{X/fast}$ and, where the dispersion relation predicts a propagating slow wave

$$X_{i+1} - X_i < \frac{1}{K_{X/slow}} \qquad \text{(d)}$$

with $K_{X/slow}$ approximated by eq. (19). As conditions (a) and (b) are in the close neighbourhood of the cyclotron resonance or its first harmonic unduely restrictive, we introduce a minimum width of a finite element given by:

$$DX_{min} = \frac{c}{\omega} \frac{\pi}{10} \sqrt{\frac{K_{\parallel_0} v_{th}}{2\omega R}}$$

so that $X_{i+1} - X_i > DX_{min}$ in any case. $2\pi \sqrt{\frac{K_{\parallel_0} v_{th}}{2R\omega}}$ is a rough estimate ot the minimal wavelength of the fast wave as it approaches a resonance.

5.3 The numerical method

Since it is not possible to apply the finite element method /11/ in its usual form to equations with non-hermitean operators, like ours, only a weak (Galerkin) variational form can be constructed. This form is obtained /12/ upon multiplying eq. (15) by an arbitrary test function $\begin{pmatrix} F_+^*(x) \\ F_-^*(x) \end{pmatrix} e^{-i(m\varphi + k_z z)}$ of some functional space and

integrating over the interval. After partial integration of terms containing second derivatives, one has:

$$\int_{x_A}^{x_B} \Big\{ \Big(1+\frac{K_{11,s}^2}{P}+2\lambda_0\Big)(\partial_-^* F_+^*)(\partial_- E_+) + (\partial_{11}^* F_+^*)(\partial_{11} E_+)$$
$$-\Big(1-\frac{K_{11,s}^2}{P}+2\lambda_0\Big)(\partial_-^* F_+^*)(\partial_+ E_-) + 2\lambda_2 (\partial_+^* F_+^*)(\partial_+ E_+)$$
$$- F_+^* L E_+ \Big\} dx = -\Big[-\frac{(1+\alpha^2)}{2} F_+^* \frac{d}{dx} E_+ + \frac{i\beta}{2} F_+^* E_+ \qquad (26)$$
$$-\Big(2\lambda_0+\frac{K_{11,s}^2}{P}\Big)\frac{u}{\sqrt{2}} F_+^* \partial_- E_+ - 2\lambda_2 \frac{u^*}{\sqrt{2}} F_+^* \partial_+ E_+$$
$$+\Big(1+2\lambda_0-\frac{K_{11,s}^2}{P}\Big)\frac{u}{\sqrt{2}} F_+^* \partial_+ E_- \Big]_{x_A}^{x_B}$$

with u given by eq. (25), and ß by (16). The second equation gives:

$$\int_{x_A}^{x_B} \Big\{ \Big(1+\frac{K_{11,s}^2}{P}+2\lambda_0\Big)(\partial_+^* F_-^*)(\partial_+ E_-) + (\partial_{11}^* F_-^*)(\partial_{11} E_-)$$
$$-\Big(1-\frac{K_{11,s}^2}{P}+2\lambda_0\Big)(\partial_+^* F_-^*)(\partial_- E_+) - F_-^* R E_- \Big\} dx \qquad (27)$$
$$= -\Big[-\Big(2\lambda_0+\frac{K_{11,s}^2}{P}\Big)\frac{u^*}{\sqrt{2}} F_-^* \partial_+ E_- - \frac{(1+\alpha^2)}{2} F_-^* \frac{d}{dx} E_-$$
$$+ i\beta/2\, F_-^* E_- + \Big(1+2\lambda_0-\frac{K_{11,s}^2}{P}\Big)\frac{u^*}{\sqrt{2}} \partial_- E_+ \Big]_{x_A}^{x_B}$$

We now use a complete set of interpolating functions $\psi_{\alpha,i}$ centered at the meshpoints X_i as test functions $F_\pm^*(X)$ and to expand $E_\pm(X)$:

$$E_\pm(X) = \sum_{i,\alpha} E_\pm^{\alpha,i}\, \psi_{\alpha,i}(X) \qquad (28)$$

For our code we have chosen cubic hermitean interpolating functions which have outstanding convergence properties. To form a complete set one needs two functions per mesh point:

$$\psi_{1,i} = \begin{cases} 0 & , X \le X_{i-1} \\ (|\xi|^2-1)(2|\xi|+1) & , X_{i-1} \le X \le X_{i+1} \\ 0 & , X \ge X_{i+1} \end{cases}$$

and $$\psi_{2,i} = \begin{cases} 0 & x \le x_{i-1} \\ (|\zeta|^2 - 1)\,(x - x_i) & x_{i-1} \le x \le x_{i+1} \\ 0 & x \ge x_{i+1} \end{cases} \quad (29)$$

where $$\zeta = \begin{cases} \dfrac{x - x_i}{x_i - x_{i-1}} & x_{i-1} \le x \le x_i \\ \dfrac{x - x_i}{x_{i+1} - x_i} & x_i \le x \le x_{i+1} \end{cases}$$

so that

$$\psi_{1,j}(x_i) = \delta_{i,j} \quad ; \quad \frac{d}{dx}\psi_{1,j}(x_i) \equiv 0$$

$$\psi_{2,j}(x_i) \equiv 0 \quad ; \quad \frac{d}{dx}\psi_{2,j}(x_i) = \delta_{i,j}$$

i.e. $E_{\pm}(X)$ and $\frac{d}{dX}E_{\pm}(X)$ are continuous. Using these functions also to interpolate $L(X)$ and (X) between mesh points we can evaluate the integrals of the left side of eq. (26) and (27) obtaining a set of linear equations for the expansion coefficients $E_{+,-}^{\alpha,i}$. The resulting "Stiffnessmatrix" is block-tridiagonal because variables at a mesh point X_i interact only with their nearest neighbours.

5.4 Boundary conditions

The right hand side of eq. (26) and (27) contains the boundary conditions. We assume that a fast wave approaches our interval from the low or high field side at a given τ with some K_z, $n\varphi$. For outgoing (transmitted or reflected) waves radiation conditions are imposed. We shall explain in the following how this has been implemented.

The E_+-component of the incoming fast wave is normalized to be one. Its polarisation $W^{inc}_{fast} = (\frac{E-}{E+})^{inc}_{fast}$ and wave vector component $K^{inc}_{X_{fast}}$ are then obtained from the dispersion relation. So are the polarisations W and the wave vector components of the outgoing fast and slow waves at both ends of the interval. Their amplitudes, $\tau_F = E_{+}{}^{tr.}_{fast}$ and $\tau_S = E_{+}{}^{tr.}_{slow}$ for transmitted and $\varrho_F = E_{+}{}^{ref}_{fast}$ and $\varrho_S = E_{+}{}^{ref}_{slow}$ for reflected waves, however, are

unknown. For these new variables we write four additional equations. If the incident fast wave comes from side A they read:

$$
\begin{aligned}
E_{+}^{1,1} &= 1 + \varrho_F + \varrho_S \\
E_{-}^{1,1} &= W_{fast}^{inc} + \varrho_F W_{fast}^{ref} + \varrho_S W_{slow}^{ref} \\
E_{+}^{1,i_{max}} &= \tau_F + \tau_S \\
E_{-}^{1,i_{max}} &= \tau_F \cdot W_{fast}^{tr} + \tau_S W_{slow}^{tr}
\end{aligned}
\qquad (30)
$$

i_{max} labeling the last mesh point. The right hand sides of eq. (26) and (27) are then expressed in terms of $\tau_F, \varrho_F, \tau_S, \varrho_S$ and the corresponding W's and K_x's replacing $\frac{d}{dx}$ by $i K_x$. In our example we would for instance have for $\frac{dE_-}{dx}|_{x_A}$:

$$
\frac{dE_-}{dx}\Big|_{x_A} = i K_{x\,fast}^{inc} W_{fast}^{inc} + i K_{x\,fast}^{ref} W_{fast}^{ref} \varrho_F + i K_{x\,slow}^{ref} W_{slow}^{ref} \varrho_S
$$

Only the contributions due to the incoming fast wave remain as "driving term" on the right hand side whereas the other waves' contributions to the boundary terms are added to the enlarged "Stiffnessmatrix".

Solving the resulting system of linear equations we get the expansion coefficients $E_{+,-}^{\alpha,i}$ as well as the amplitudes $\tau_{S,F}$ and $\varrho_{S,F}$ of the outgoing waves. In the next subchapter we shall show how to obtain from these quantities the powerfluxes of the corresponding waves.

5.5 The power balance

Conservation of energy is a trivial consequence of eq. (26) and (27). Upon replacing $F_+^*(X)$ by $E_+^*(X)$, adding the two equations and taking the imaginary part we obtain the power balance /12/:

$$\int_{X_A}^{X_B} Q(X)\, dx = P \Big|_{X_A}^{X_B} \tag{31}$$

Q(X) denotes the differential power absorbed by the plasma per unit length due to the various damping processes. In particular we have

$$\begin{aligned} Q^{ICD} &= \mathrm{Im}(L)\,|E_+|^2 + 2\,\mathrm{Im}(\mathcal{Z}_2)\,|\partial_+ E_+|^2 \\ Q^{TTMP} &= 2\,\mathrm{Im}(\mathcal{Z}_0)\,|\partial_- E_+ - \partial_+ E_-|^2 \\ Q^{ELD} &= \mathrm{Im}\left(\frac{K_{\parallel,s}^2}{P}\right)\cdot|\partial_- E_+ + \partial_+ E_-|^2 \end{aligned} \tag{32}$$

On the other hand, P is the sum of the power fluxes of the transmitted fast and slow waves or of the incoming fast and reflected fast and slow waves. All these quantities are easily evaluated using the various $\mathcal{Z}$'s and $\mathcal{S}$'s and the corresponding W's and K_X's. After numerical integration, eq. (31) can serve as a first consistency check of our code.

5.6 Convergence properties

In order to investigate the convergence properties of our numerical method we have made test runs varying the number of mesh points N. As test parameters A(N) we have chosen $A_{1,2} = |E_+|^2\ (X_{1,2})$ at two positions $X_{1,2}$, one where the slow wave is evanescent, one where it is propagating and $A_3 = E^{ions}_{abs,max}$, the maximum differential power absorbed by ions per unit length. The "true" values $A_i\ (\infty)$ have been estimated by extrapolation. Fig. 2 shows plots of $\log\left(\frac{A_i(N) - A_i(\infty)}{A_i(\infty)}\right)$ versus log N. As scenario we have taken a plasma with a He_3^{++} minority in H^+ which requires particularly good resolution because of the short wavelength of the shear Alfvén wave. We find that the convergence of $|E_+|^2$ scales like N^{-5}, that of $E^{ions}_{abs,max}$ like N^{-3} in accordance with the results from other authors /12/.

6. Applications

Although our code is fast enough to make possible the incorporation into a ray tracing code we have run it in the following examples as individual package. The plasma and tokamak parameters have been chosen to by typical for a JET discharge: B = 3.5 Tesla, B^{Pol}/B_{tor} = 0.1, R_T = 300 cm. If not explicitely statet, we have used: $T_e = T_i$ = 2 keV. The fast wave is assumed to be launched from the low magnetic field side (LMFS). We have considered three different heating scenarios:

a. Pure first harmonic heating of a D^+-plasma; ν = 50 MHz, $n_e = 5 \cdot 10^{13} cm^{-3}$. fig. 3 shows $\mathcal{L}_2(X)$ and the position of the confluence between fast and Bernstein wave as given by eq. (23). The Bernstein wave is propagating at the HMFS. We have investigated the case of an incoming fast wave in the equatorial plane ($\vartheta \equiv$ o) with $K_Z = 0$ and toroidal mode number n_φ = 10. The electric field predicted by the code is depicted in fig. 4, the power balance is given in table 1. ($R_{S,F}$ denotes the power fluxes of reflected, $T_{S,F}$ of transmitted slow and fast waves; $E_{abs,i}$ the total power absorbed by the ion species i and E_{TTMP}, E_{ELD} the total power absorbed by electrons due to TTMP and ELD. All these quantities are normalized to the incoming power.)
In fig. 4 the ion Bernstein wave to the left of the resonance is clearly visible. In spite of its large amplitude it transports only 3.6 % of the incoming power. This is due to its partially electrostatic polarisation which is, however, not enough for efficient ELD. (For $K_Z = 0$, $\vartheta = 0$ eq. (13) gives a rather small $K_{\parallel,S} = \frac{n_\varphi}{R_o} \cdot \cos\Theta$.) This shows the limits of a 1-d model. In a tokamak the slow wave is diffracted as it propagates towards regions of shorter wavelength and this will enhance its subsequent absorption by ELD. Nevertheless the lack of absorption in our model indicates that power deposition to electrons could be appreciably broader than usually admitted. We have also calculated absorption and power fluxes as function of the ion temperature T_i (fig. 5). As expected, absorption increases with temperature.

b. H^+-minority in D^+ at $\omega = \Omega_{c_H} = 2\,\Omega_{c_D}$; other parameters as in example a.

Figure 6 shows $\lambda_2(X)$ and $L(X)$ as well as the evanescence layer between the positions of resonance and cut-off of the fast wave for 3 % H^+ in a deuterium plasma. In fig. 7 we have plotted the e.m. field for a run with $\tau = 0$, $n_\varphi = 10$, $K_Z = 0$. For the same reason as in case a., ELD of the Bernstein wave, which is excited at the ion-ion hybridresonance near R = 312 cm, is negligible. Figure 8 shows the results of the power balance as function of the angle of incidence, i.e. of K_Z ($K_Z = \pm\ 0.27\ cm^{-1}$ corresponds to an incoming fast wave making an angle of $\pm$ 45° relative to the resonance layer). Since $K_\parallel$ is proportional to K_Z, absorption increases with K_Z. For $K_Z = -\ 0.32\ cm^{-1}$ $K_\parallel$ nearly vanishes.

A more systematic comparison of the predictions of our code with the estimates used in ray tracing is made in fig. 9 which shows the power balance under the same conditions as above (with $K_Z = 0$) varying the H^+-concentration. For $n_H + \simeq 0.05 \cdot n_e$ the power absorbed by ions remains nearly constant since the mode conversion layer lies outside the Doppler broadened cyclotron resonance of the minority. At this concentration the transition from the minority to the mode conversion regime occurs /3/.

Using the n_φ-spectrum of the JET quadrupole and dipole antennae, as obtained from a numerical code /13/, we have also calculated the deposition profiles in the equatorial plane ($\tau \equiv 0$) by superposing the contributions of each toroidal mode n_φ limiting ourselves to waves with $K_Z = 0$ (fig. 10 and 11). For the quadrupole antenna we find a broader absorption profile since its spectrum is shifted towards larger n_φ values compared to the spectrum of the dipole antenna. The results of the total power balance for all toroidal modes are listed in table 2. (For the dipole antenna all terms add up to 96.5 % since our code can not treat the $n_\varphi = 0$ mode which contributes the missing 3.5 % of the total power launched by the antenna.)

c. He_3^{++} minority in a H^+-plasma at $\omega \simeq \Omega_{c_{He_3^{++}}}$; ν = 35.6 MHz, $n_e = 8 \cdot 10^{13}$ cm^{-3}.

Figure 12 shows a plot of L(X) as well as the evanescence layer between the cut off and the (isolated) ion ion hybrid resonance of the fast wave for 3 % He_3^{++} in a H^+-plasma. Figure 13 shows a run with $n_\varphi = 10$, $K_z = 0$, $\tau = 1.5$ rad. In this case, FLR terms are negligible near the wave resonance and the cold plasma shear Alfvén wave is excited. This wave propagates towards the LMFS away from the IC resonance of He_3^{++} and is accurately electrostatic, hence unaffected by TTMP. The strong absorption visible in fig. 13 is entirely due to ELD, which is very important in this region where $\tau \simeq \pi/2$.

Figure 14 shows the corresponding power deposition profile proving that TTMP affects only the fast and ELD only the slow wave. The modulation in Q_{ELD} is due to the interference of the slow wave with the incoming and reflected fast waves. The spatial average of Q_{ELD}, however, depends only on the slow wave's amplitude. The power balance for this example is given in table 3. In order to compare our results with those from semianalytical models, we have run the code without ELD and TTMP. Figure 15 shows the power balance as function of the He_3^{++} concentration (all other parameters as above) together with the analytical approximations /3/. Taking into account that in the analytical model the absorbed power is attributed to the power coupled to the reflected slow wave, the two curves are in excellent agreement.

Table 1

R_F = 2.2 %
R_S = 0. %
T_F = 78.4 %
T_S = 3.6 %
E_{abs,D^+} = 15.8 %
E_{TTMP} E_{ELD} 0.1 %

Table 2

dipole antenna	quadrupole antenna
$E_{abs,ionen}$ = 50.0 %	$E_{abs,ionen}$ = 66.4 %
$E_{abs,el}$ = 2.3 %	$E_{abs,el}$ = 5.0 %
R_F = 29.9 %	R_F = 8.2 %
T_F = 11.3 %	T_F = 19.2 %
T_S = 3.0 %	T_S = 1.1 %

Table 3

$E_{abs,He_3^{++}}$ = 0.9 %
E_{ELD} = 21.5 %
E_{TTMP} = 3.1 %
R_F = 39.6 %
R_S 0.1 %
T_F = 34.8 %

References

/1/ M.Brambilla, Ray Tracing of Lower Hybrid and Ion Cyclotron Waves, 3rd Europ. Workshop on Problems in the Numerical Modelling in Plasma, Varenna 1985 (to be published in J. Comp. Phys. 1986); further references therein.

/2/ F.W.Perkins, Nucl. Fusion 17, 1197, 1977.

/3/ M.Brambilla, M.Ottaviani, Plasma Phys. and Contr. Nucl. Fusion 27, 1, 1985.

/4/ D.G.Swanson, Proc. 3rd Int. Symp. on Heating in Toroidal Plasma, Grenoble 1982, Vol. 1, p. 285.

/5/ P.L.Colestock, R.J. Kashuba, Nucl. Fusion 23, 763, 1983.

/6/ M.Brambilla, M.Ottaviani, Plasma Phys. and Contr. Fusion, 27, 919, 1985.

/7/ Budden, Radio Waves in the Ionosphere, Chp. 21, Cambridge Univ. Press, 1955.

/8/ M.Brambilla, IPP 4/209, November 1982.

/9/ B.D.Fried, S.D. Conte, The plasma dispersion function, Academic Press, New York 1961.

/10/ R.R.Weynants, Phys. Rev. L-tt. 33, 78, 1974.

/11/ S.Strang, G.J.Fix, Analysis of the Finite Element Method, Prentice Hall 1973.

/12/ K.Appert, T.Hellsten, J.Vaclavik, L.Villard, Lausanne-Report LRP 268/85.

/13/ M.Brambilla, private communication.

A summary of this report will be published in the Proceedings of the 13th Europ. Conf. on Contr. Fusion and Plasma Heating, Schliersee, 1986.

Figure Captions

Fig. 1: Modeling resonance layers in a tokamak in one dimension.

Fig. 2: Convergence properties; plots of the relative deviations $(A_i(N) - A_i(\infty))/A_{i(\infty)}$ of three quantities A_1 versus the number of finite elements N.

Fig. 3: Plot of $\lambda_2(X)$ for heating of a single species (D^+) Plasma at the second harmonic; ν = 50 MHz, $n_e = 5 \cdot 10^{13}$ cm^{-3}; T = 2 keV; n_φ = 10.

Fig. 4: Solution of the corresponding wave equation for $\tau = 0$, $K_Z = 0$. Shown is the E_+-component of the e.m. field.

Fig. 5: Plot of the power balance as function of the ion temperature T_i; other parameters as above.

Fig. 6: Plots of $\lambda_2(X)$ and L(X) for 3 % H^+ in a D^+-plasma; other parameters as in fig. 3.

Fig. 7: Solution of the wave equation for $\tau = 0$, $K_Z = 0$. Shown are the E_+- and E_--components.

Fig. 8: Power balance as function of K_Z, other parameters as above.

Fig. 9: Power balance as function of n_{H^+} for $K_Z = 0$.

Fig. 10: Deposition profile in the equatorial plane ($\tau = 0$) for the JET-dipole antenna ($K_Z = 0$).

Fig. 11: Deposition profile in the equatorial plane ($\tau = 0$) for the JET-quadrupole antenna ($K_Z = 0$).

Fig. 12: Plot of L(X) for 3 % He_3^{++} in a H^+-plasma; ν = 35.6 MHz; $n_e = 8 \cdot 10^{13}$ cm^{-3}; T_i = 2 keV; n_φ = 10.

Fig. 13: Solution of the corresponding wave equation for $K_Z = 0$, $\mathcal{L} = 1.5$ rad.

Fig. 14: Power deposition profile for the above case.

Fig. 15: Power balance as function of $n_{He_3}{}^{++}$ without TTMP, ELD. Other parameters as above.
Results from our code (left) and from a semi-analytical model (right).

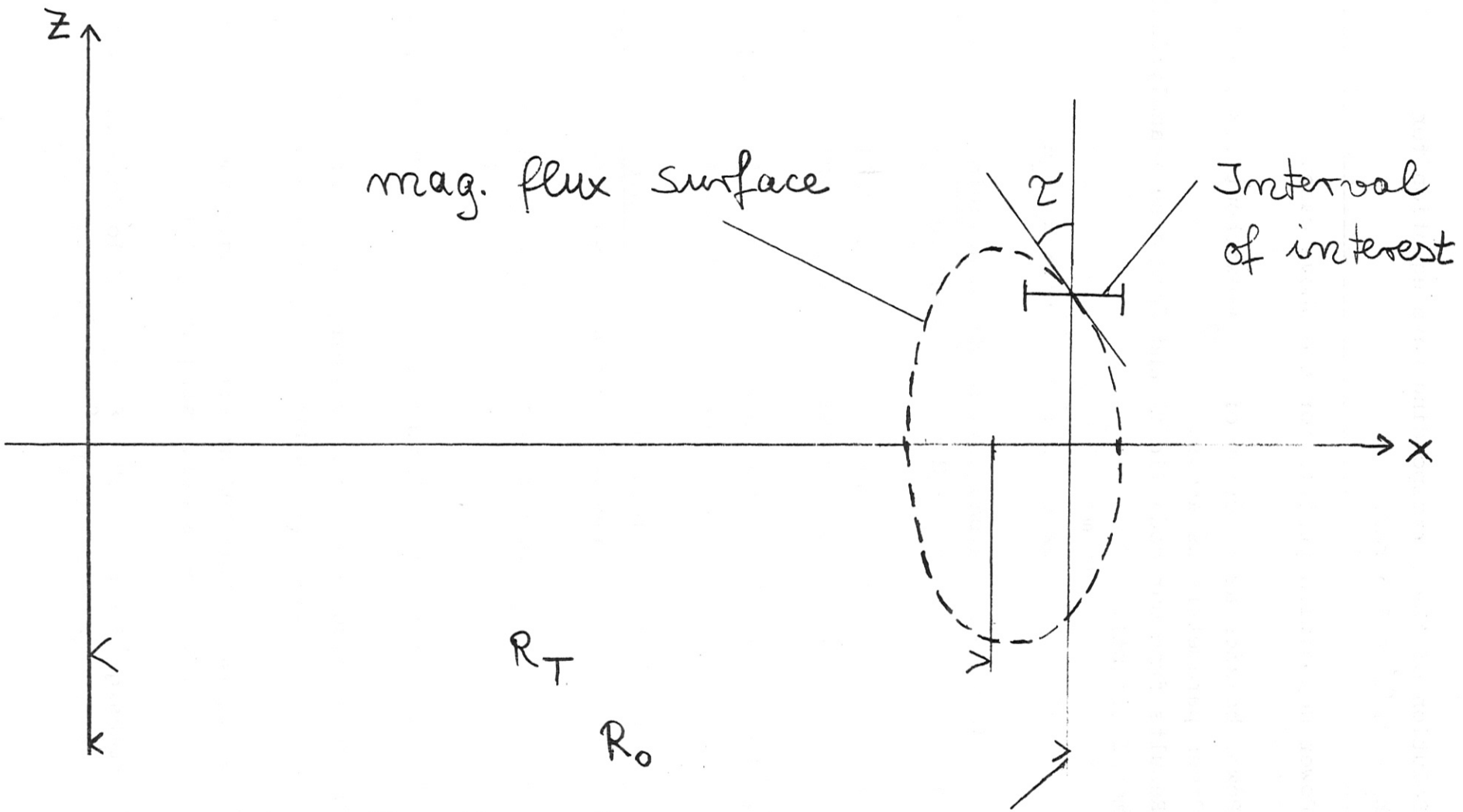
Z
mag. flux surface
χ
Interval
of interest
X
R_T
R_0
Position of cyclotron resonance
($\omega = \Omega_{ci}$ or $\omega = 2\Omega_{ci}$)

Fig. 6

Fig 2

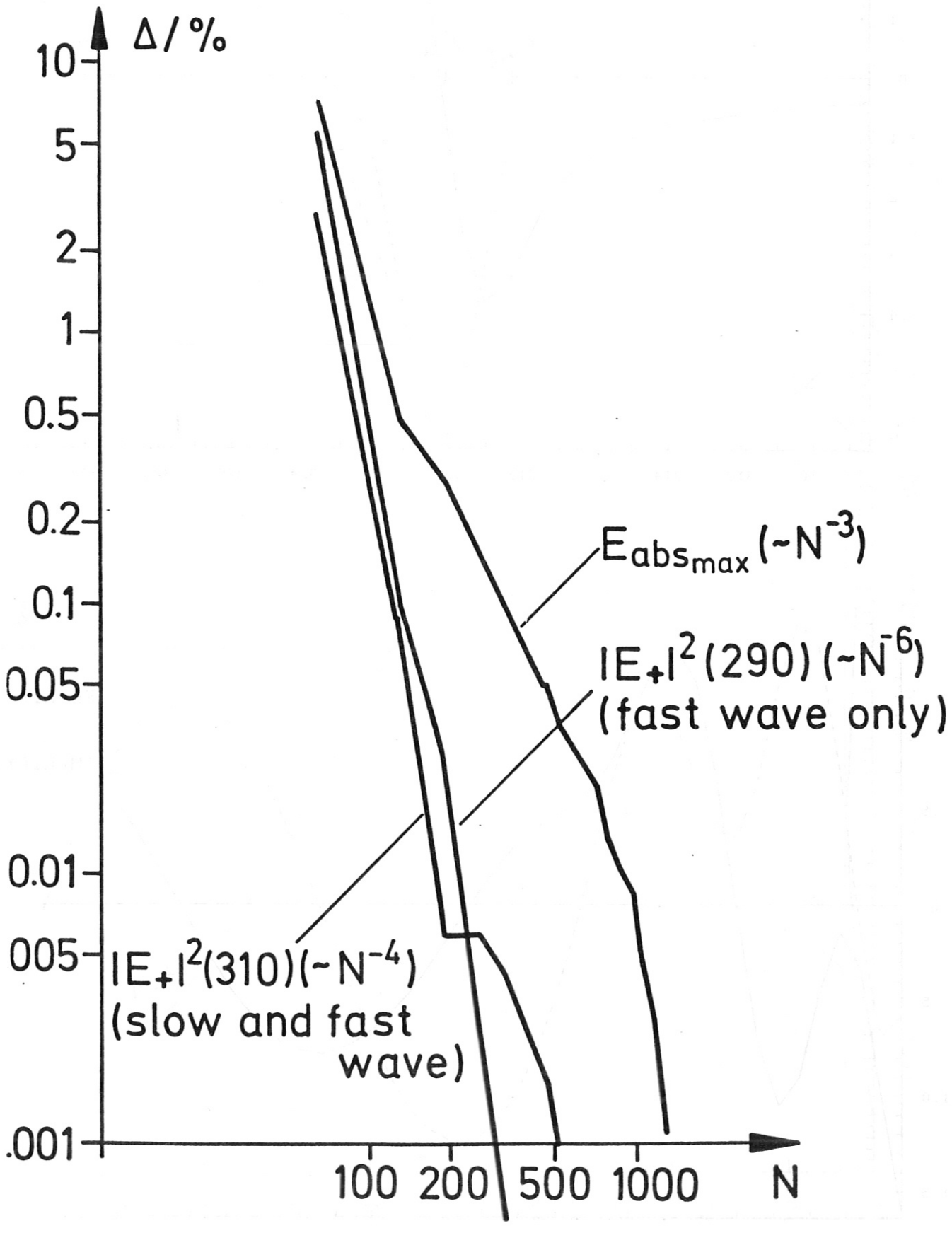
Δ / %
10
5
2
1
0.5
0.2
0.1
0.05
0.01
005
.001
$E_{abs_{max}}$ (~N^{-3})
$|E_+|^2$(290) (~N^{-6})
(fast wave only)
$|E_+|^2$(310)(~N^{-4})
(slow and fast
wave)
100 200 500 1000
N

Fig 3

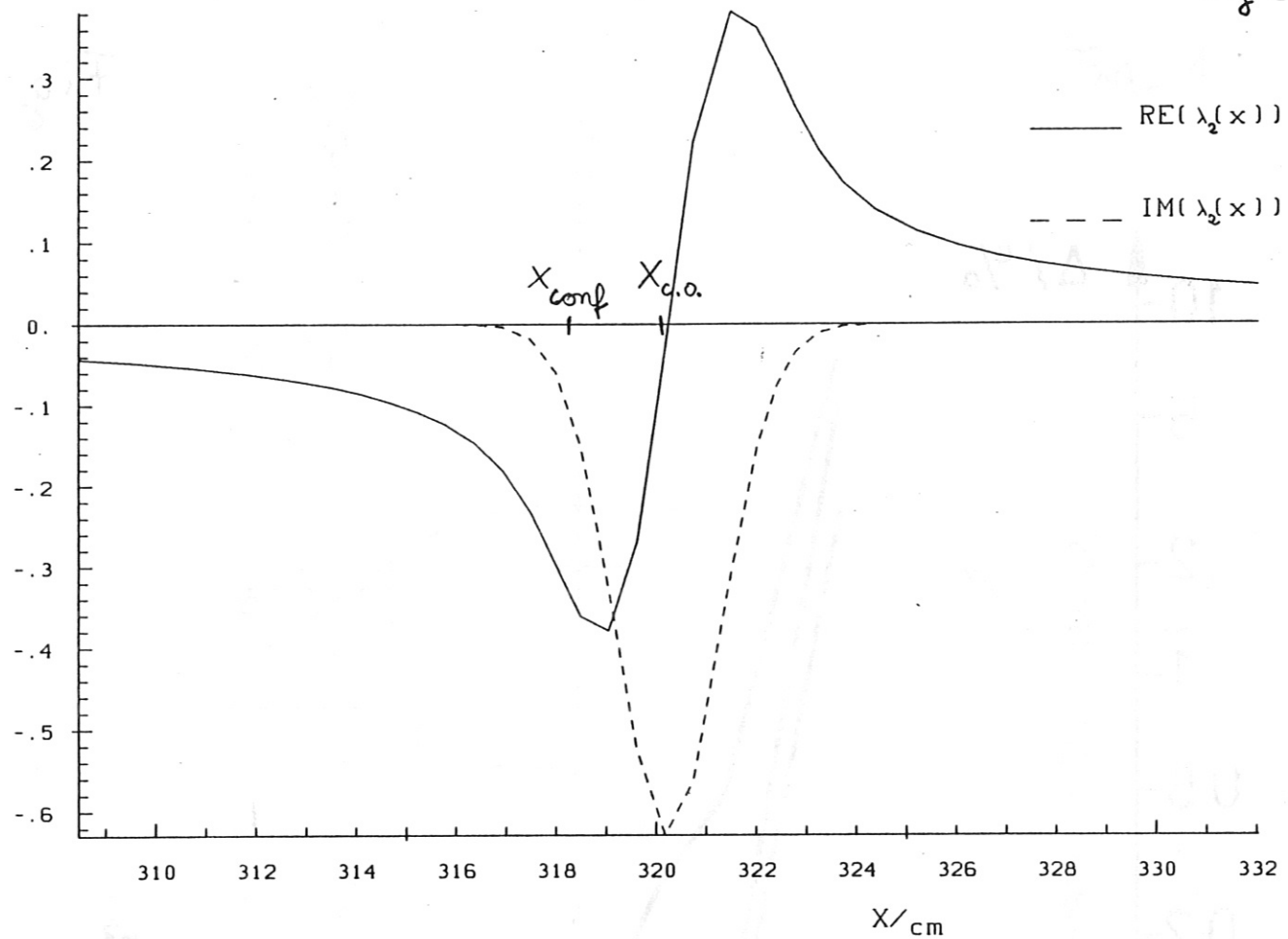
RE(λ2(x))
IM(λ2(x))
Xconf
X c.o.
.3
.2
.1
0.
-.1
-.2
-.3
-.4
-.5
-.6
310
312
314
316
318
320
322
324
326
328
330
332
X/cm

Fig. 4

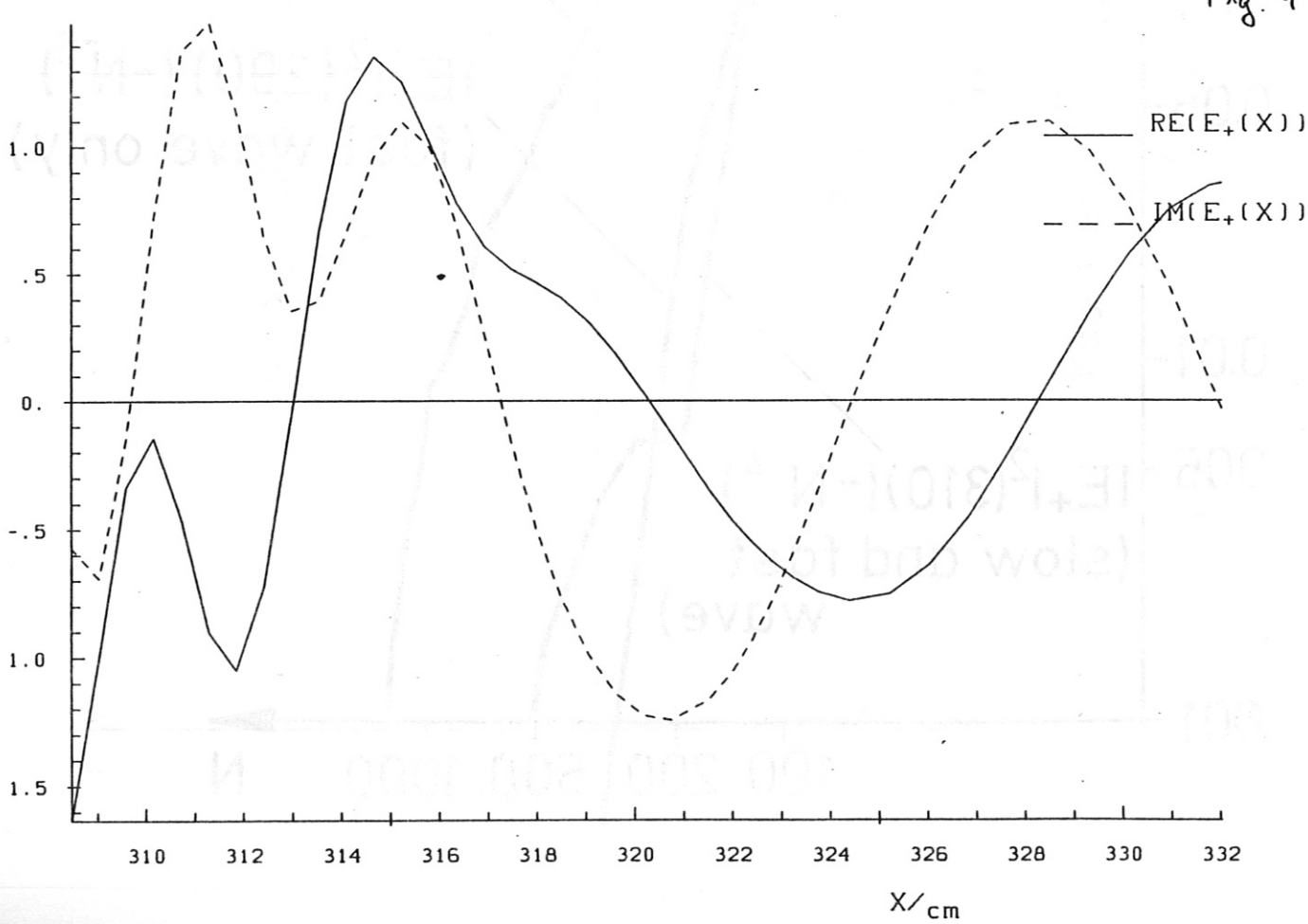
RE(E+(X))
IM(E+(X))
1.0
.5
0.
-.5
1.0
1.5
310
312
314
316
318
320
322
324
326
328
330
332
X/cm

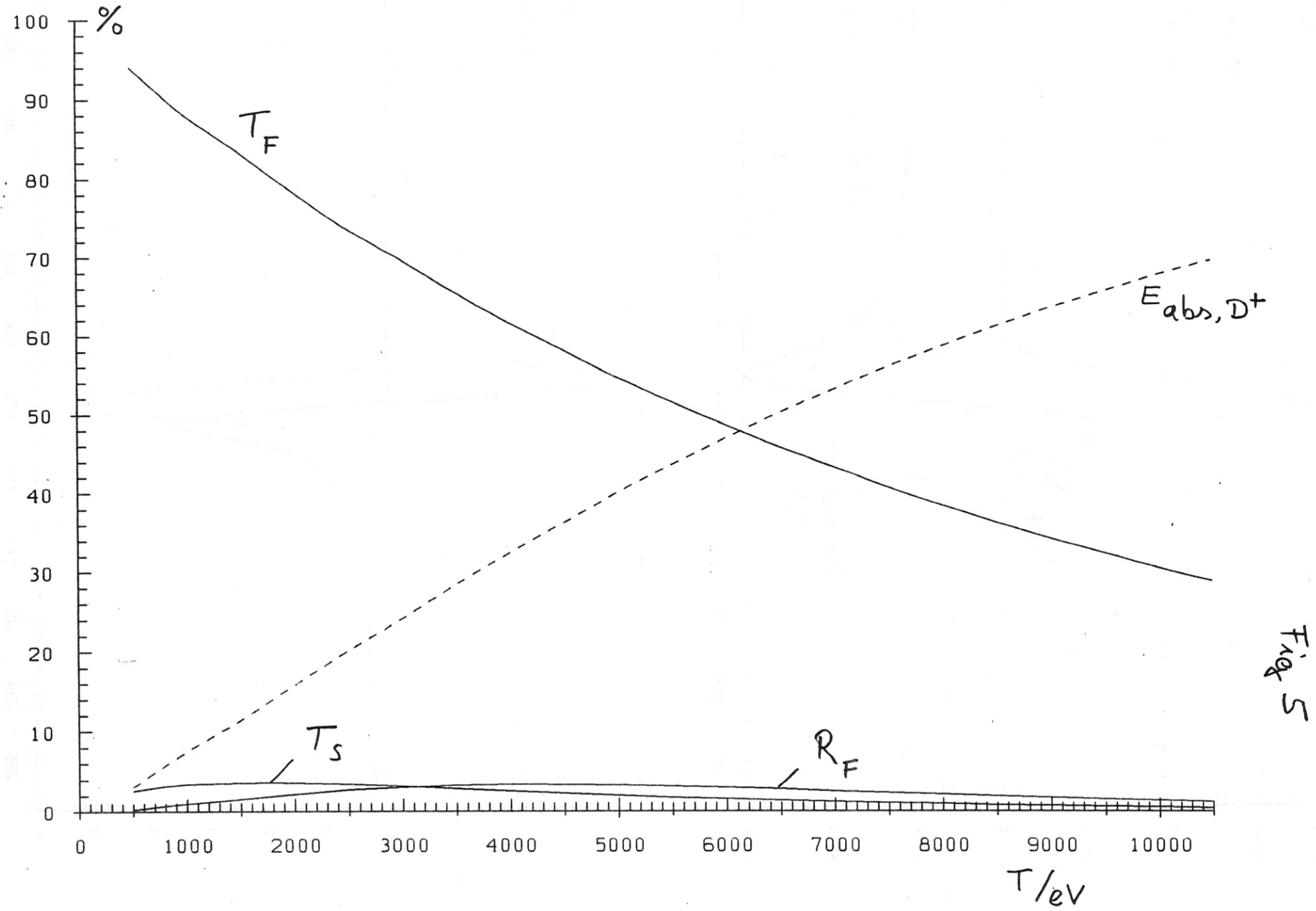
100
%
90
80
70
60
50
40
30
20
10
0
T_F
E_{abs,D^+}
T_S
R_F
0
1000
2000
3000
4000
5000
6000
7000
8000
9000
10000
T/eV

Fig. 5

Fig 6

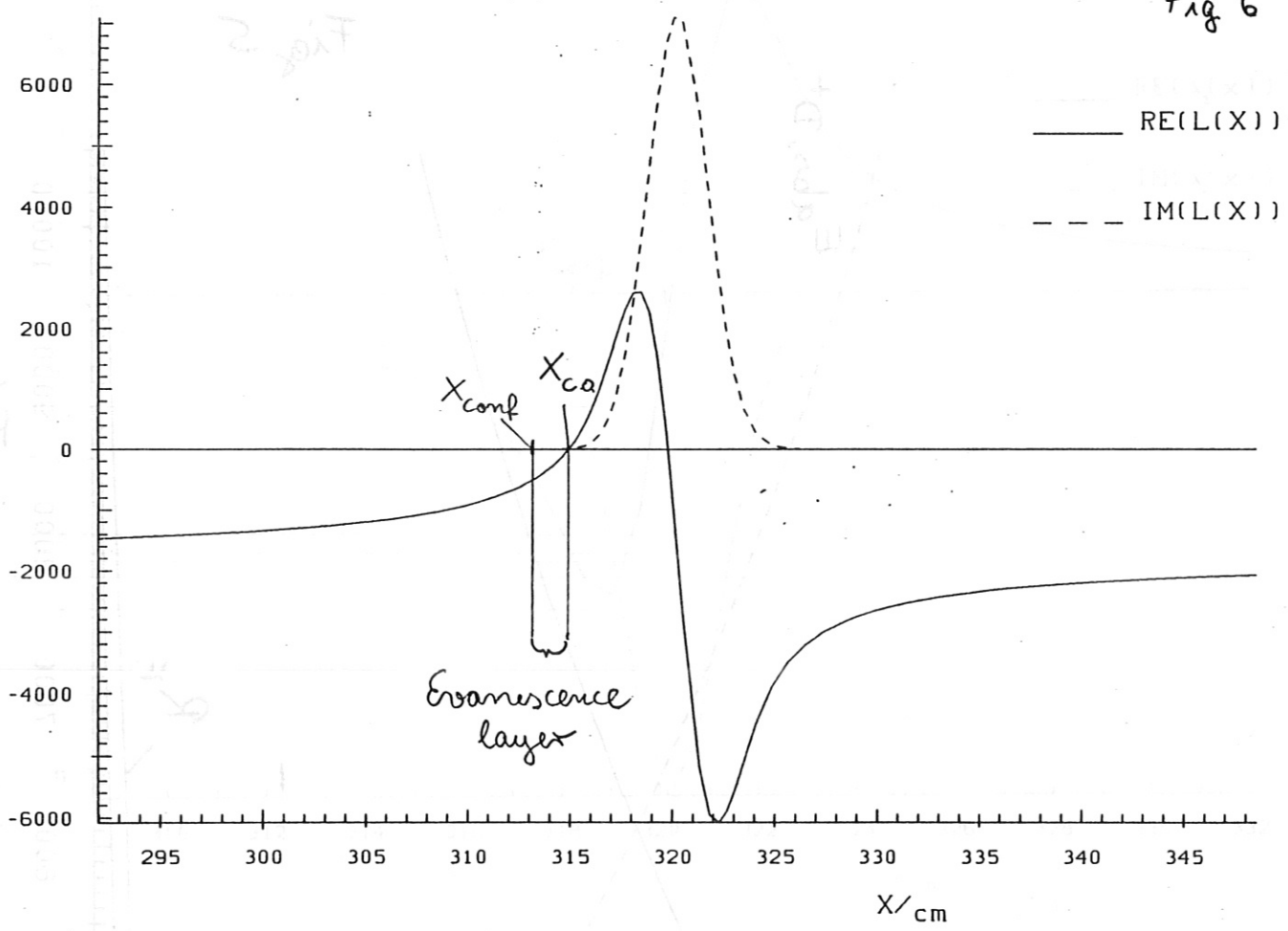
6000
4000
2000
0
-2000
-4000
-6000
RE(L(X))
IM(L(X))
X_{conf}
X_{ca}
Evanescence layer
295
300
305
310
315
320
325
330
335
340
345
X/cm

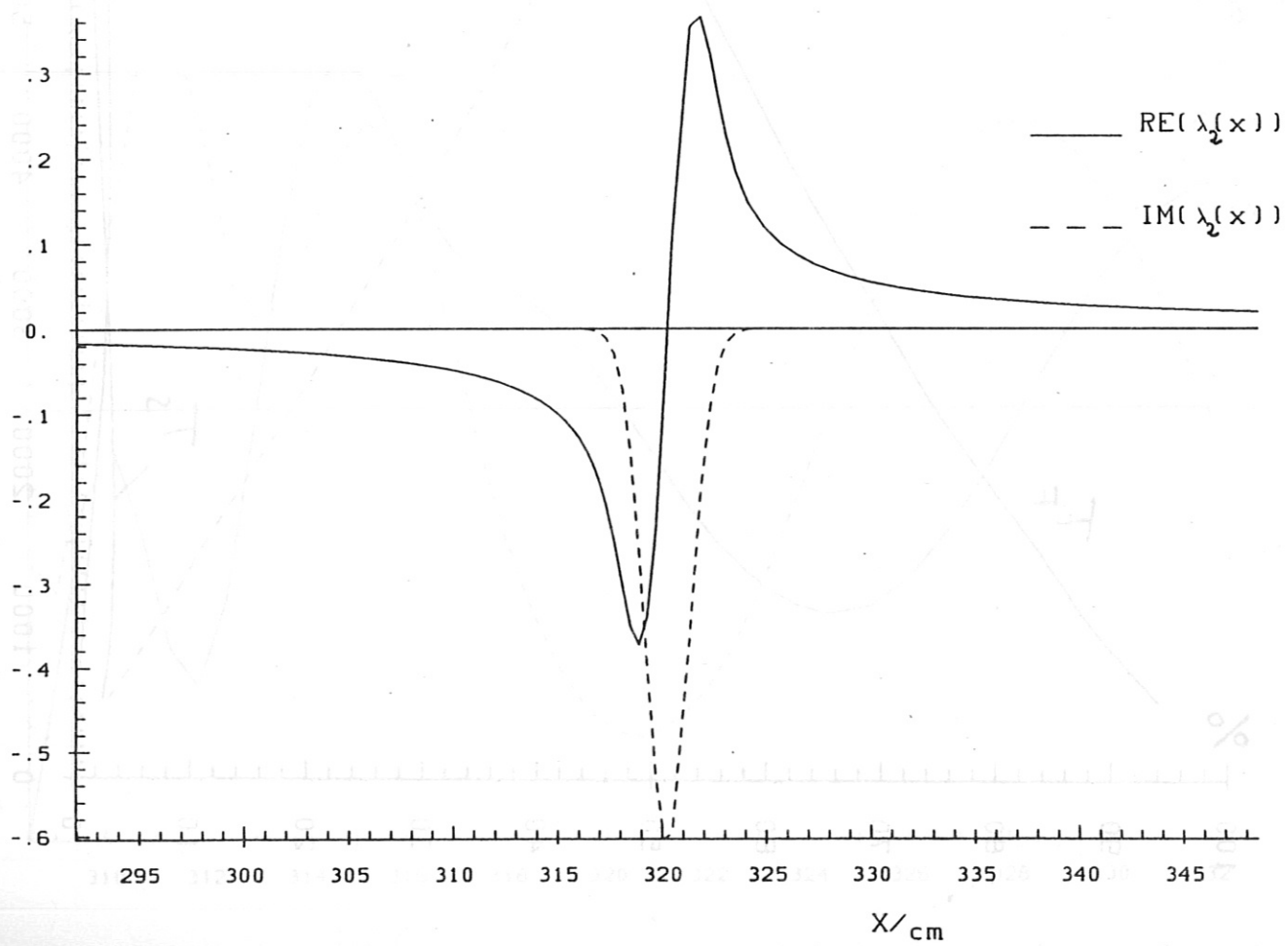
.3
.2
.1
0.
-.1
-.2
-.3
-.4
-.5
-.6
RE(λ_2(x))
IM(λ_2(x))
295
300
305
310
315
320
325
330
335
340
345
X/cm

Fig 7

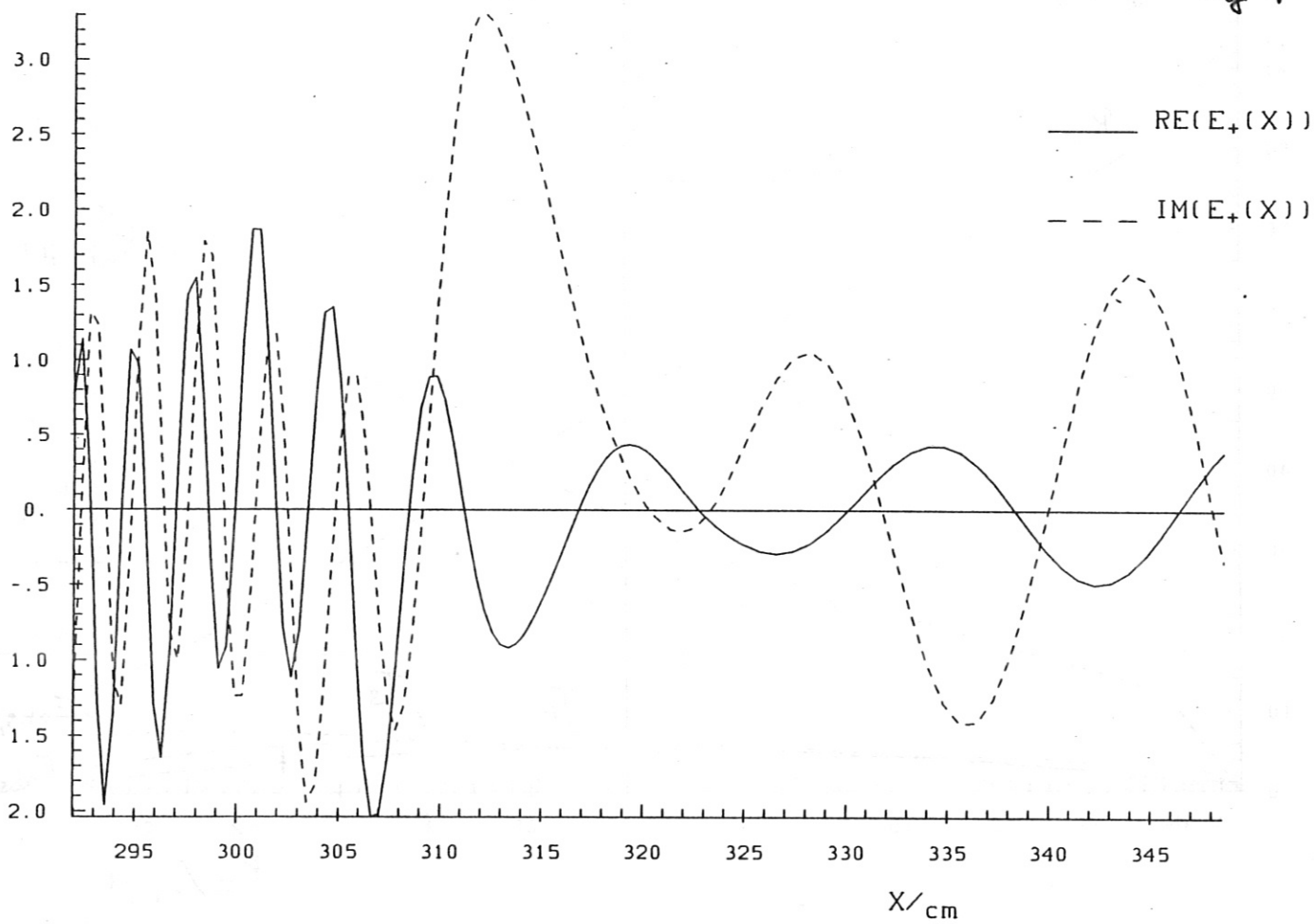
3.0
2.5
2.0
1.5
1.0
.5
0.
-.5
1.0
1.5
2.0
295
300
305
310
315
320
325
330
335
340
345
X/cm
RE(E+(X))
IM(E+(X))

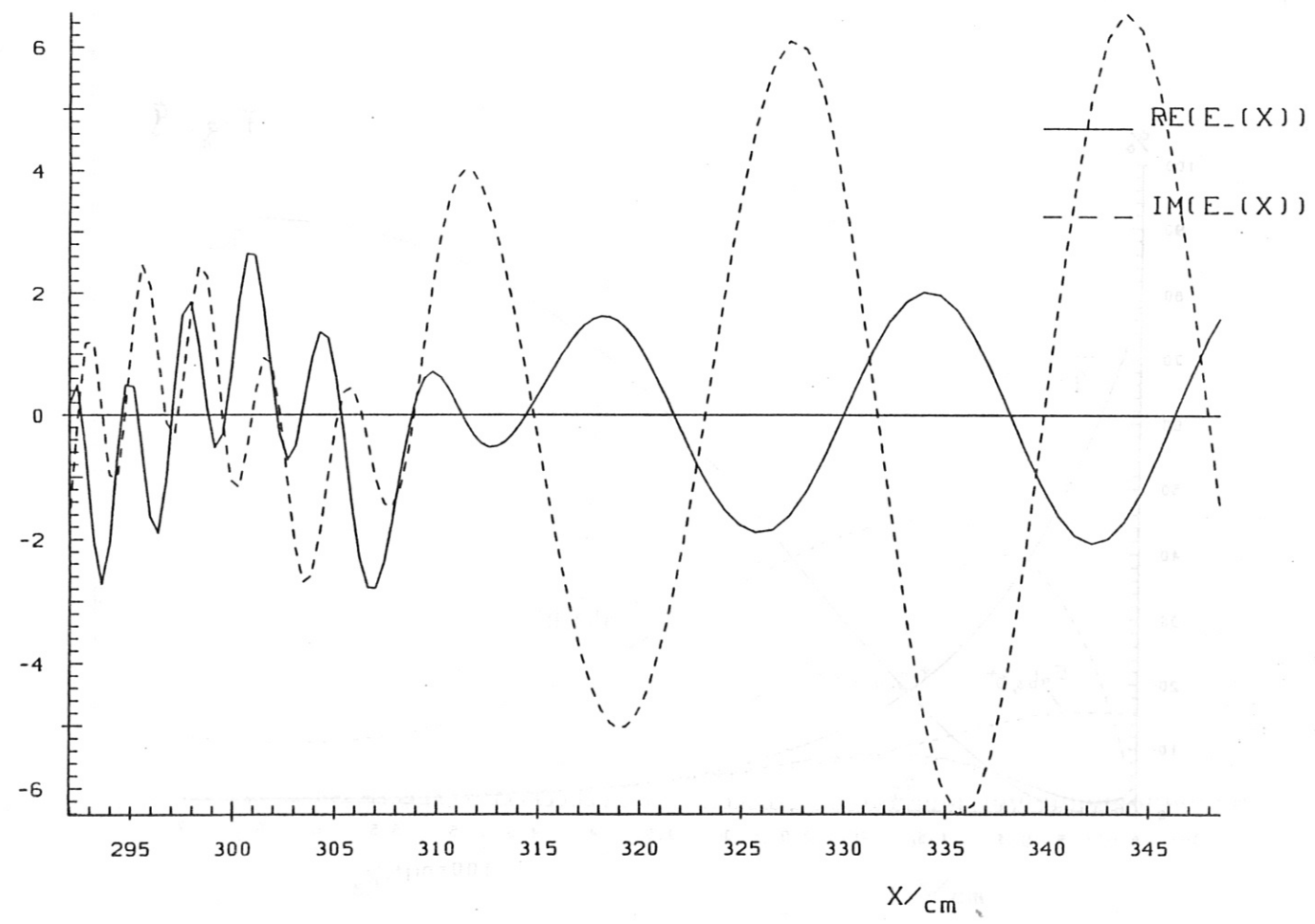
6
4
2
0
-2
-4
-6
295
300
305
310
315
320
325
330
335
340
345
X/cm
RE(E-(X))
IM(E-(X))

Fig 8

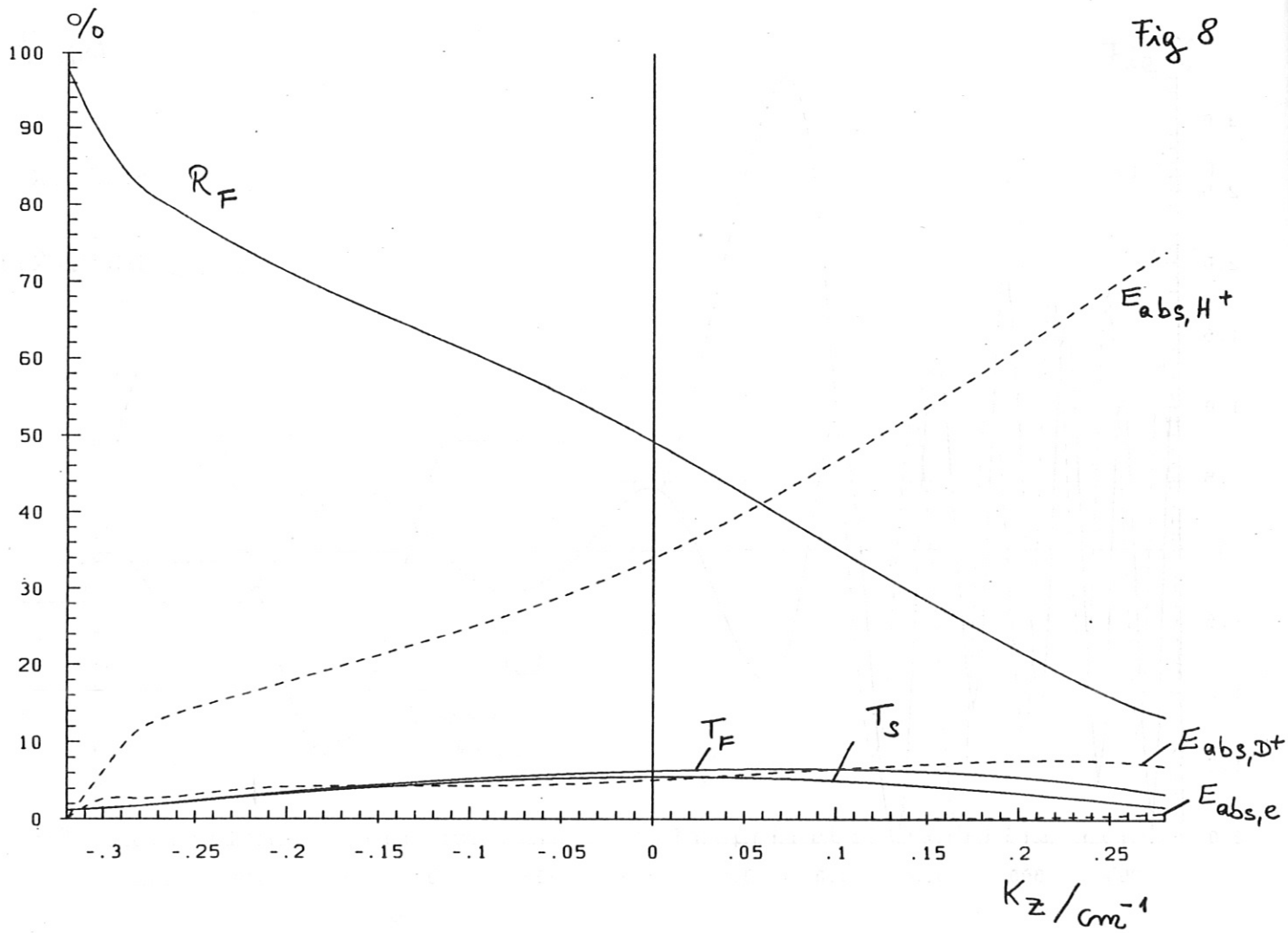
%
100
90
80
70
60
50
40
30
20
10
0
R_F
E_{abs,H^+}
T_F
T_S
E_{abs,D^+}
$E_{abs,e}$
-.3
-.25
-.2
-.15
-.1
-.05
0
.05
.1
.15
.2
.25
K_z / cm^{-1}

Fig. 9

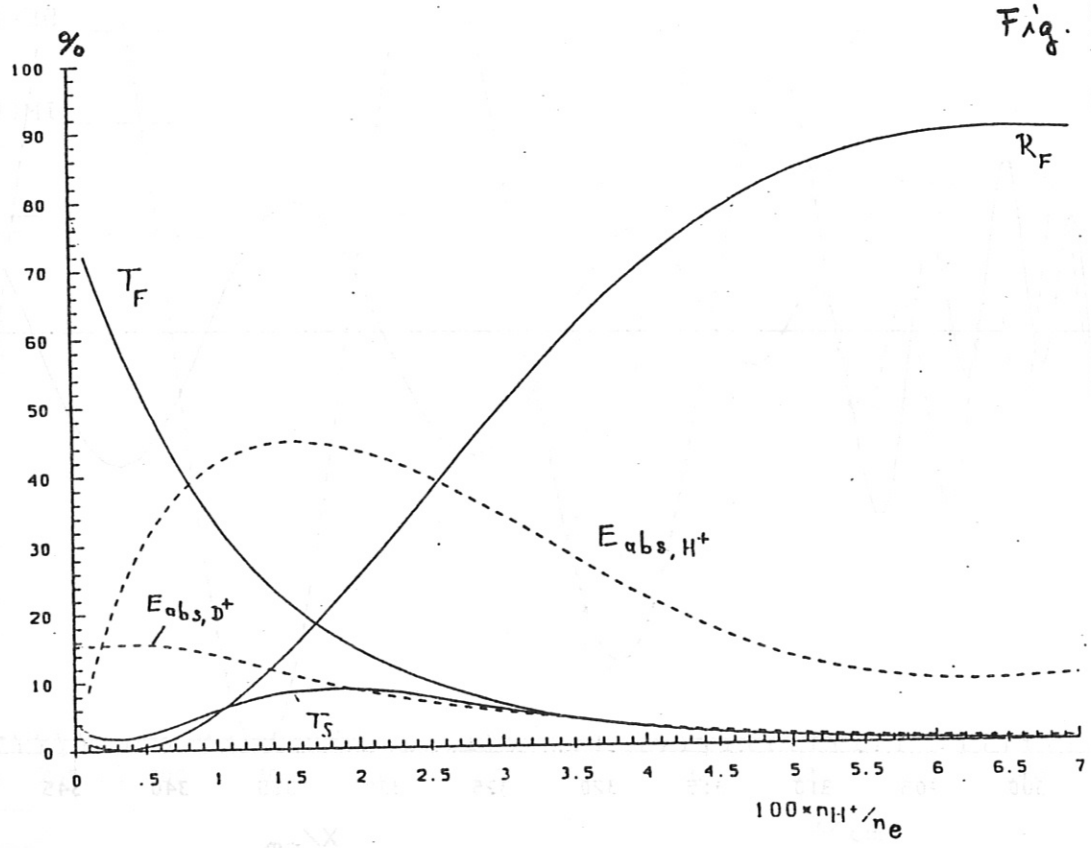
%
100
90
80
70
60
50
40
30
20
10
0
R_F
T_F
E_{abs,H^+}
E_{abs,D^+}
T_S
0
.5
1
1.5
2
2.5
3
3.5
4
4.5
5
5.5
6
6.5
7
$100 \times n_{H^+} / n_e$

Fig 10

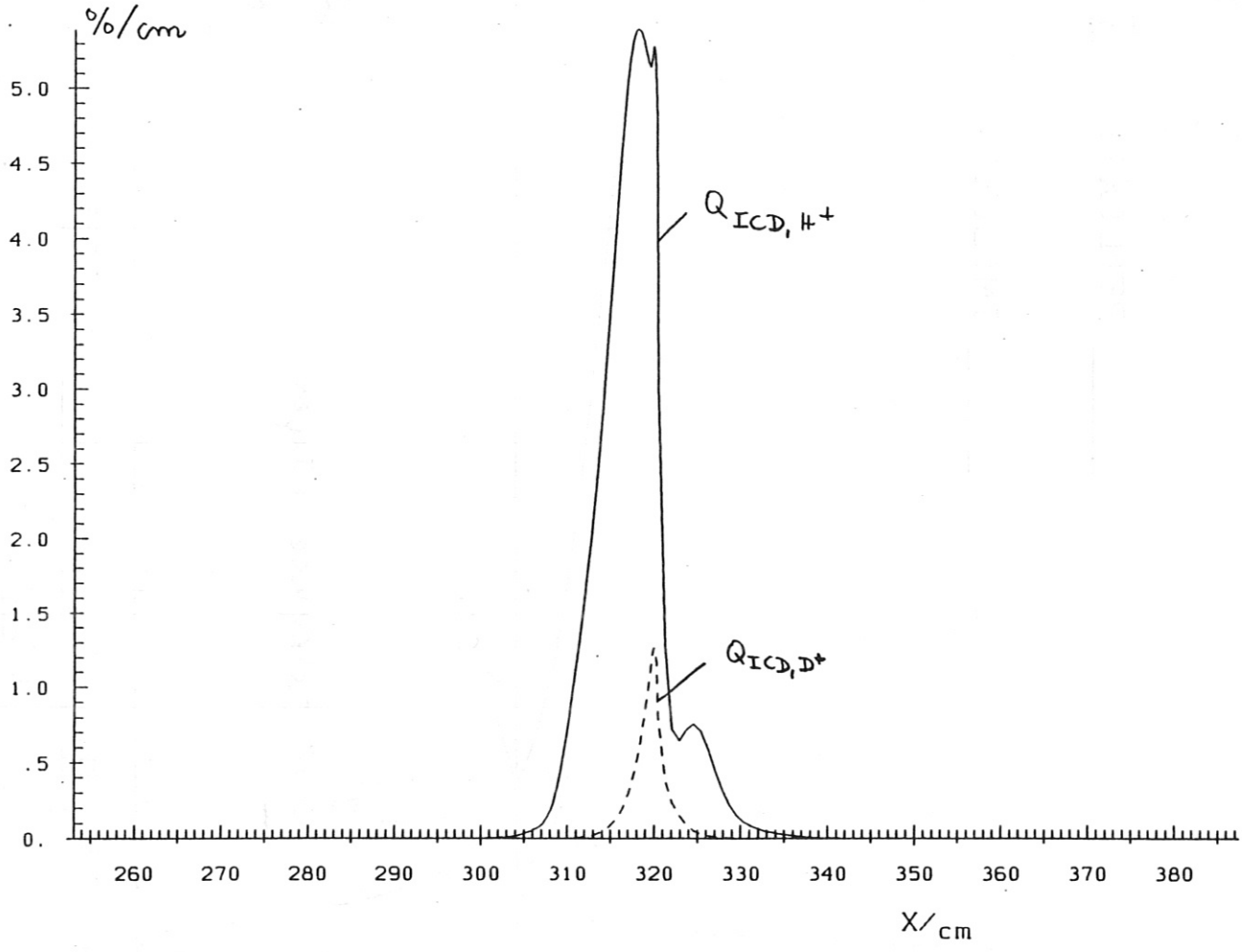
%/cm
5.0
4.5
4.0
3.5
3.0
2.5
2.0
1.5
1.0
.5
0.
Q_{ICD,H^+}
Q_{ICD,D^+}
260
270
280
290
300
310
320
330
340
350
360
370
380
X/cm

Fig 11

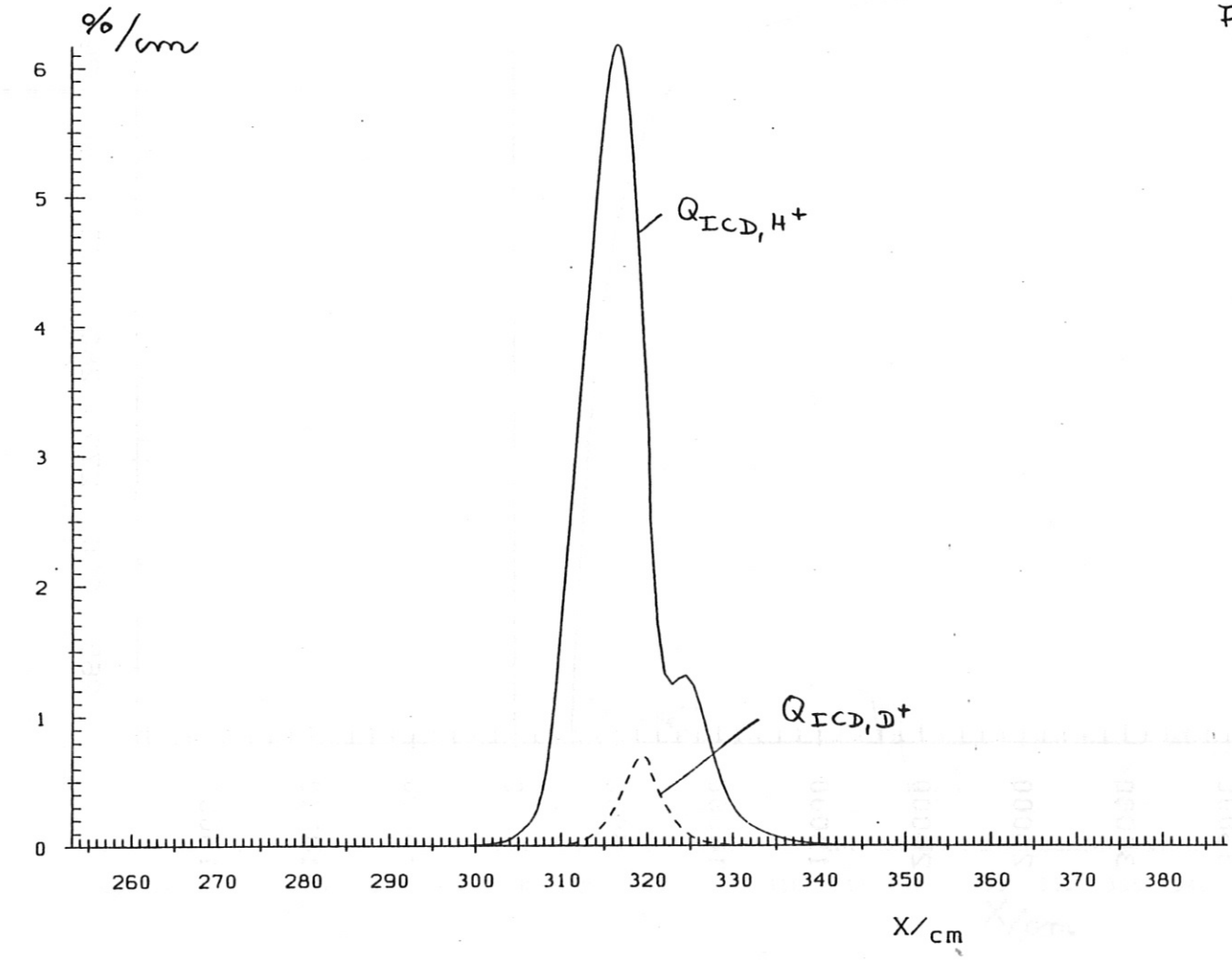
%/cm
6
5
4
3
2
1
0
Q_{ICD,H^+}
Q_{ICD,D^+}
260
270
280
290
300
310
320
330
340
350
360
370
380
X/cm

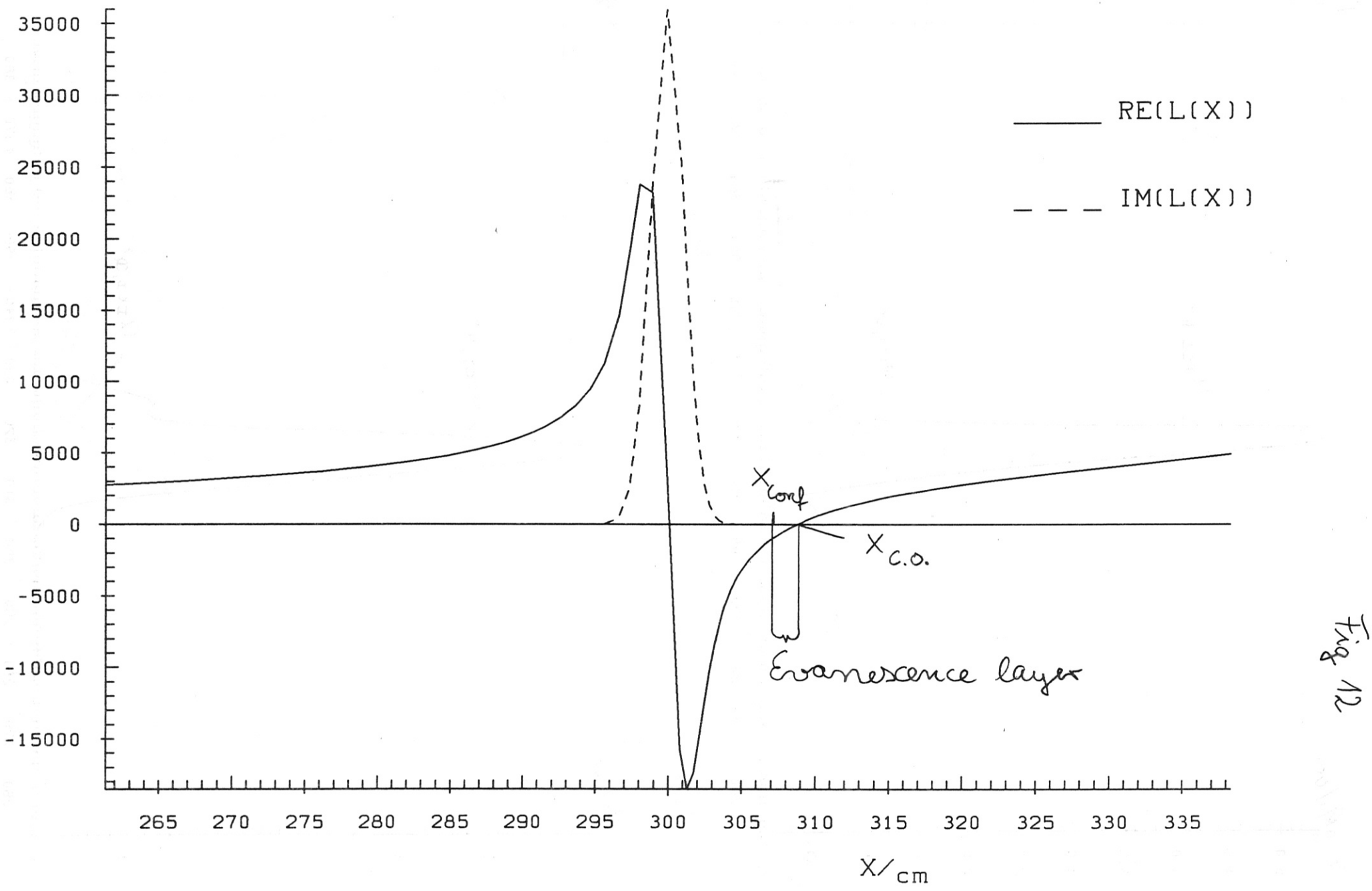
35000
30000
25000
20000
15000
10000
5000
0
-5000
-10000
-15000
265
270
275
280
285
290
295
300
305
310
315
320
325
330
335
X/cm
RE(L(X))
IM(L(X))
X conf
X c.o.
Evanescence layer

Fig 12

Fig 13

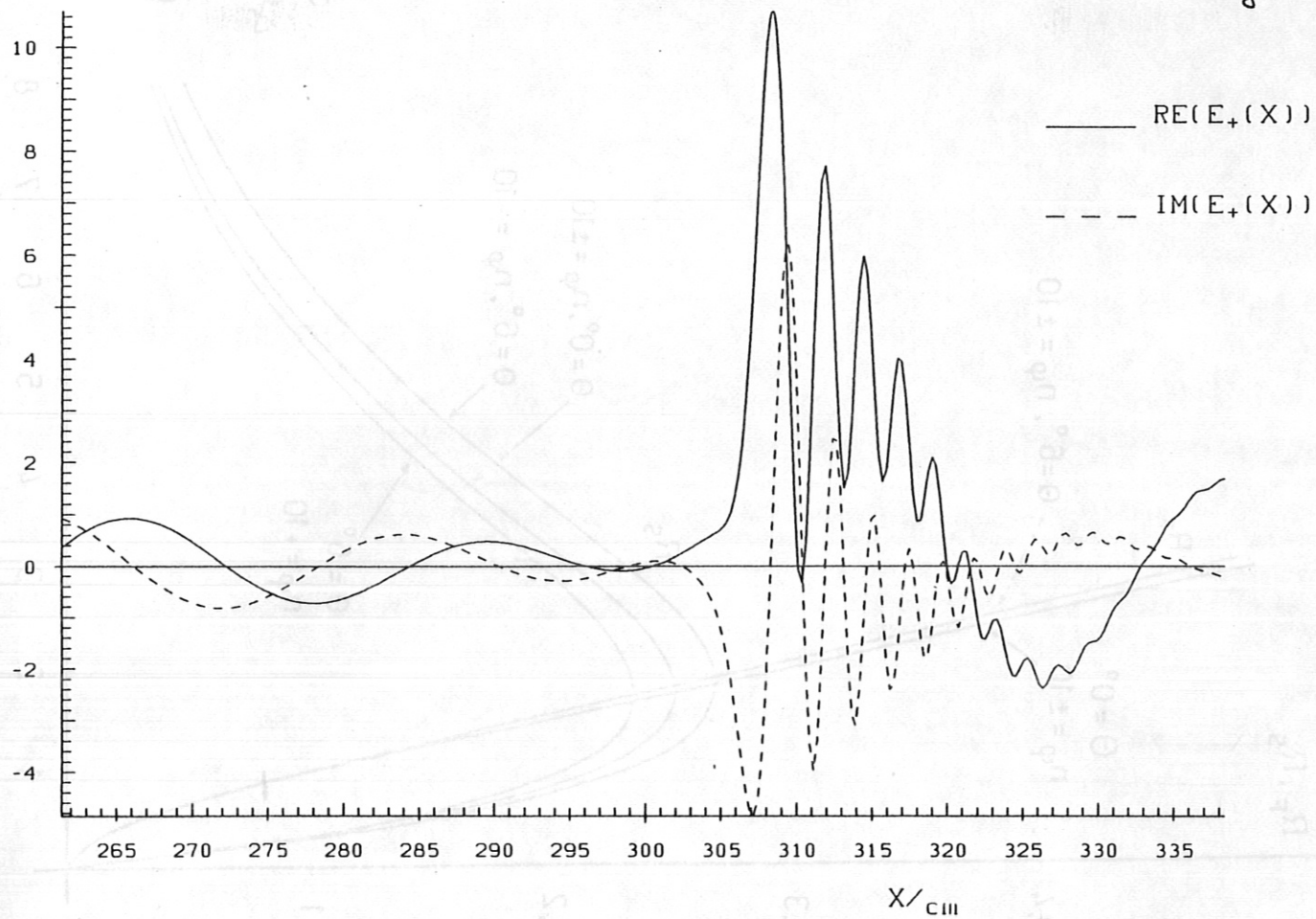
RE(E+(X))
IM(E+(X))
10
8
6
4
2
0
-2
-4
265 270 275 280 285 290 295 300 305 310 315 320 325 330 335
X/cm

Fig 14

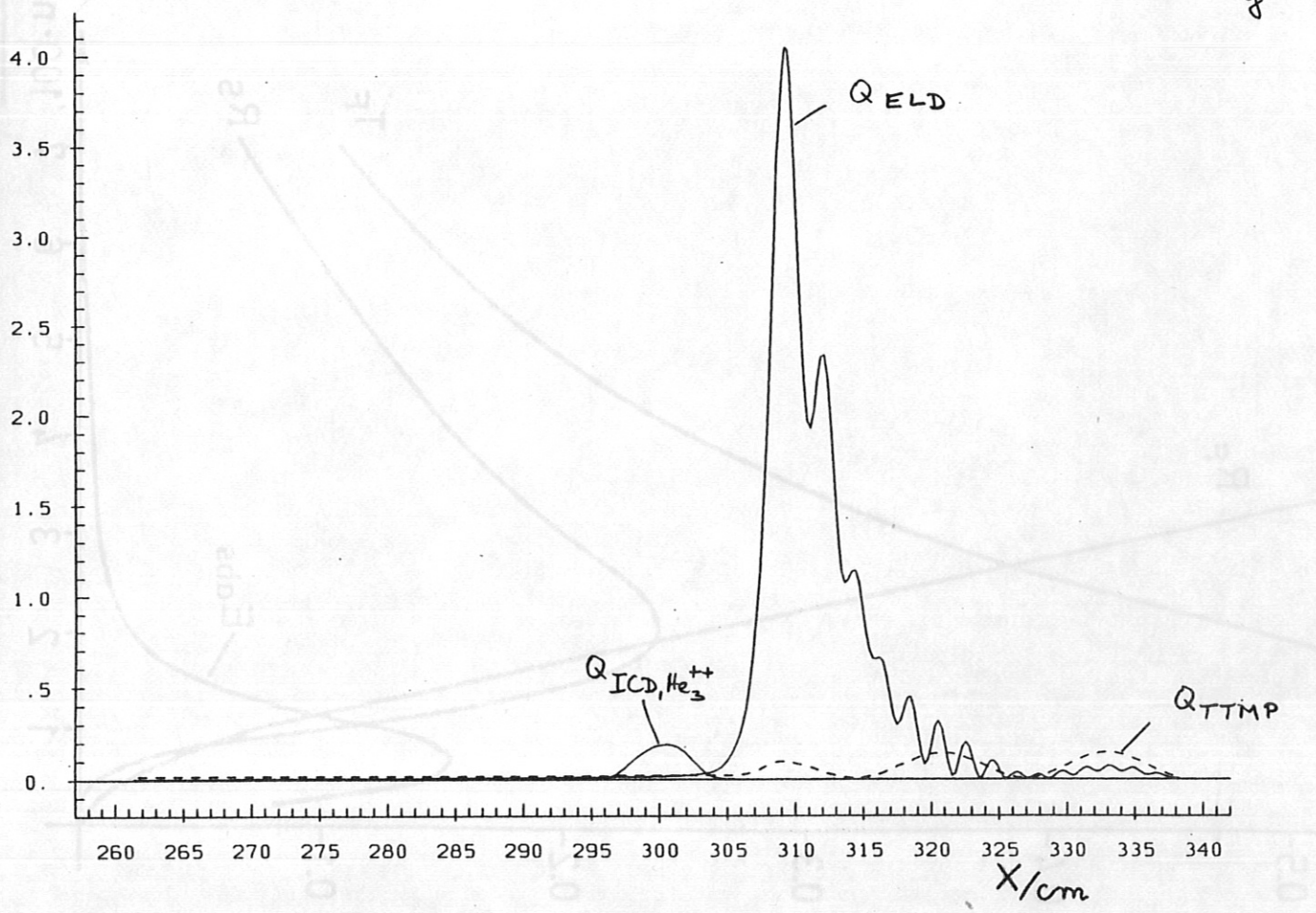
Q ELD
Q ICD, He3++
Q TTMP
4.0
3.5
3.0
2.5
2.0
1.5
1.0
.5
0.
260 265 270 275 280 285 290 295 300 305 310 315 320 325 330 335 340
X/cm

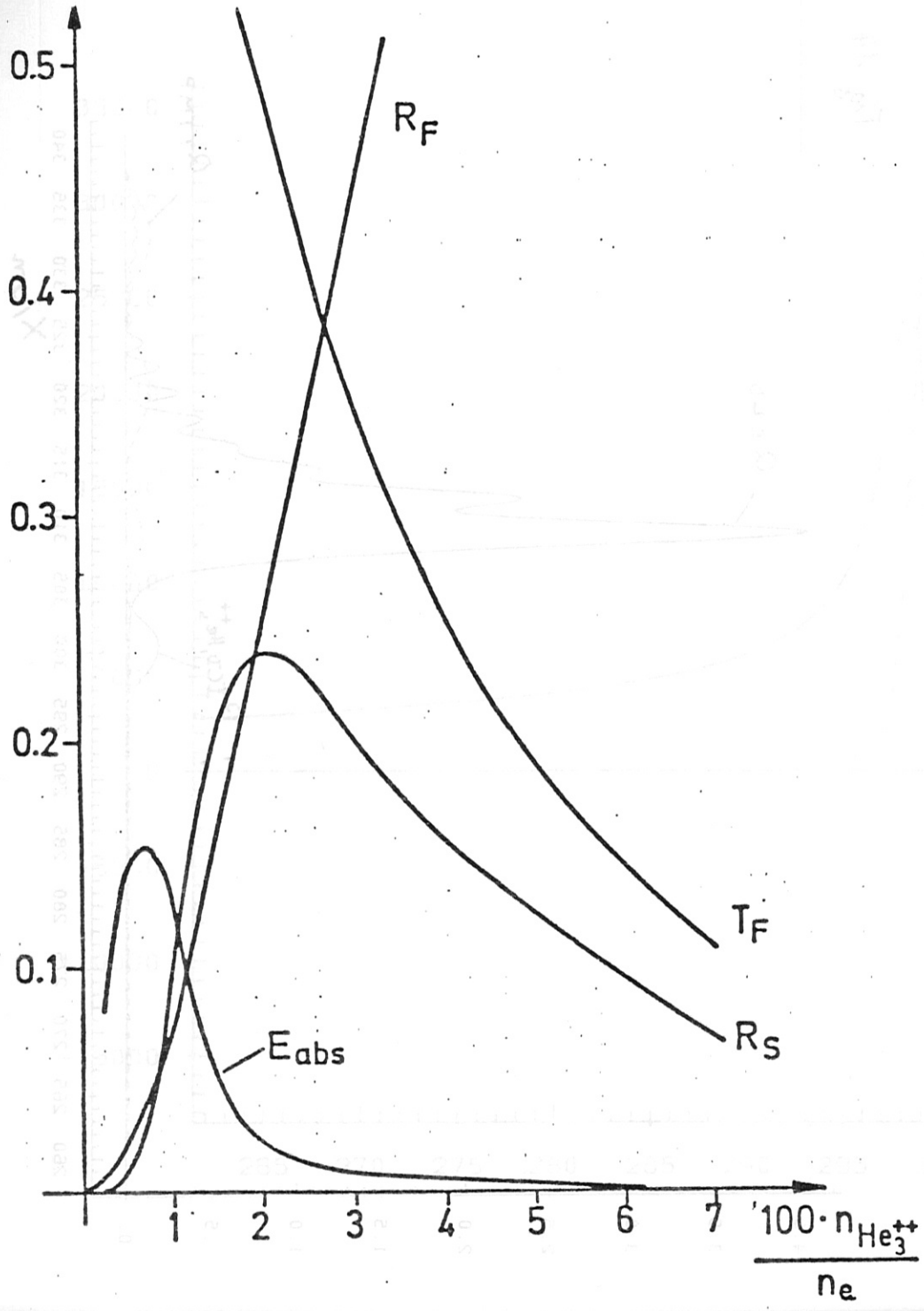
0.5
0.4
0.3
0.2
0.1
R_F
T_F
R_S
E_{abs}
1
2
3
4
5
6
7
$100 \cdot n_{He_3^{++}} / n_e$

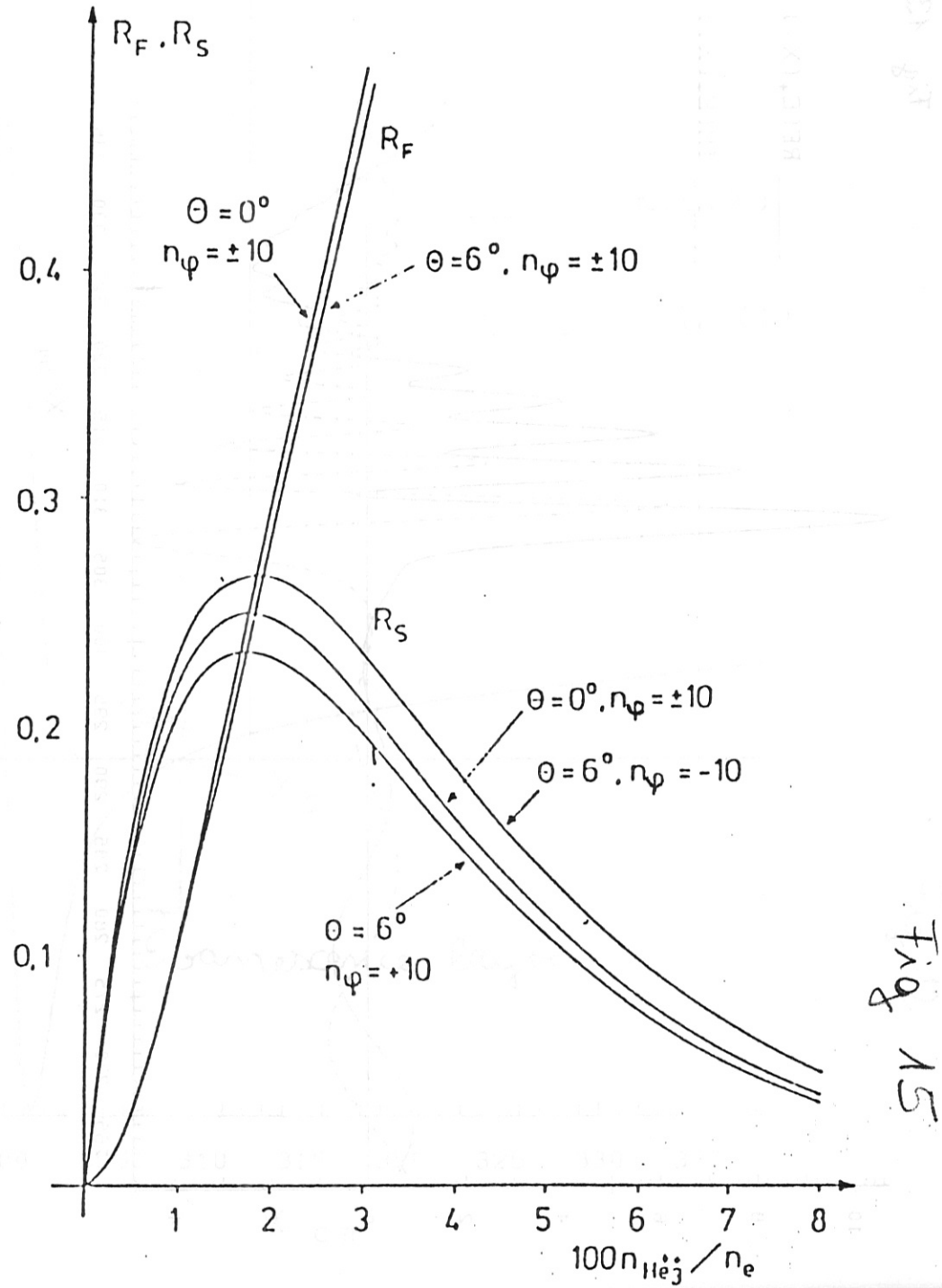
R_F, R_S
R_F
$\Theta = 0°$
$n_\varphi = \pm 10$
$\Theta = 6°, n_\varphi = \pm 10$
0.4
0.3
0.2
0.1
R_S
$\Theta = 0°, n_\varphi = \pm 10$
$\Theta = 6°, n_\varphi = -10$
$\Theta = 6°$
$n_\varphi = +10$
1
2
3
4
5
6
7
8
$100 n_{He_3^{++}} / n_e$